University of Tennessee, Knoxville
TRACE: Tennessee Research and Creative Exchange

Masters Theses | Graduate School

5-2005

Ametropic Eye Modeling

Bo Tan
University of Tennessee - Knoxville

Follow this and additional works at: https://trace.tennessee.edu/utk_gradthes

 Part of the Physics Commons

Recommended Citation

Tan, Bo, "Ametropic Eye Modeling. " Master's Thesis, University of Tennessee, 2005.
https://trace.tennessee.edu/utk_gradthes/2363

This Thesis is brought to you for free and open access by the Graduate School at TRACE: Tennessee Research and Creative Exchange. It has been accepted for inclusion in Masters Theses by an authorized administrator of TRACE: Tennessee Research and Creative Exchange. For more information, please contact trace@utk.edu.

To the Graduate Council:

I am submitting herewith a thesis written by Bo Tan entitled "Ametropic Eye Modeling." I have examined the final electronic copy of this thesis for form and content and recommend that it be accepted in partial fulfillment of the requirements for the degree of Master of Science, with a major in Physics.

Ying-Ling Chen, Major Professor

We have read this thesis and recommend its acceptance:

James W.L. Lewis, Horace W. Crater

Accepted for the Council:
Carolyn R. Hodges

Vice Provost and Dean of the Graduate School

(Original signatures are on file with official student records.)

To the Graduate Council:

I am submitting herewith a thesis written by Bo Tan entitled "Ametropic eye modeling." I have examined the final electronic copy of this thesis for form and content and recommend that it be accepted in partial fulfillment of requirements for the degree of Master of Science, with a major in Physics.

Ying-Ling Chen
Major Professor

We have read this thesis
and recommend its acceptance:

James W.L. Lewis

Horace W. Crater

Accepted for the Council:

Anne Mayhew
Vice Chancellor and
Dean of Graduate Studies

(Original signatures are on file with original student records.)

AMETROPIC EYE MODELING

A Thesis

Presented for the

Master of Science

Degree

The University of Tennessee, Knoxville

Bo Tan

May, 2005

Acknowledgements

I would like to take this opportunity to thank all those who made this thesis possible. First, thanks to Dr. Ying-Ling Chen for her guidance and patience all the time in the research. I would also like to express my appreciation to my committee members, Dr. Ying-Ling Chen, Dr. James W.L. Lewis and Dr. Horace W. Crater for their assistance in getting this thesis in its final form. Here I especially want to express my thankfulness to them for their help and care in my study and life since I came to U.S. I also would like to thank Dr. Ying-Ling Chen, Dr. James W.L. Lewis, Dr. Horace W. Crater, Dr. Christian G. Parigger, Dr. L. M. Davis and Dr. Marianne Breinig for helping in my physics courses. I would like to thank all my family and friends for their moral support through the years.

Abstract

Using a commercial optical design software, a general ametropic eye model was constructed based on the measured data of 69 young adults. The experiment data was obtained from 2 published literatures. The correlation between refractive errors of the eyes and their axial lengths, cornea curvatures and intraocular powers was investigated and adopted into the modeling for the first time. The optical performance of the new model eye was evaluated and compared with published aberration data from human eyes. The comparison was performed on both on-axis and periphery vision. High-order wavefront aberrations that include the asymmetric properties of eyes and the correlation of high-order aberrations with refractive error were also discussed.

Contents

List of Figures

Chapter1

Introduction to eye modeling

A current research activity of the University of Tennessee Space Institute (UTSI) Center for Laser Applications (CLA) is the development and application of ocular instruments for telemedicine. Of particular interest is the design and use of ophthalmic devices that will be applicable to the screening of vision function of subjects who are located in medically under-served regions. A specific objective is to perform this screening function using simply operated devices and computer-based analysis. For this purpose, use will be made of fundus reflection of incoherent illumination of the eye. It is desired that quantitative performance predictions be a central feature of the design and performance of the measurement apparatus and methods and that post-fabrication empirical modifications be minimized. To be able to achieve this, it is essential that accurate optical computations be performed for the range of ophthalmic conditions that can be expected for the anticipated population sample. Of course, these calculations include the response of the eye and the device to the external illumination source that is used for the examination. Further, the application environment of the screening function can be either clinical or not, and the desired simplicity of operation requires that pupil dilation not be required. Because of this necessity of non-cycloplegic measurements (refer to Appendix

I), the pupil diameter of the eye can range from that appropriate to a paraxial optical description to a wide-angle ocular irradiation case. This thesis concentrates on the determination of the ocular response to such an illumination stimulus and measurement environment. Central to this task is the analytic model one uses for the optical performance of the eye. In this work, an assessment and review are given of previously described and used optical models of the eye, and new computations and analysis are performed to propose an improved eye model for our application goal.

The functions and workings of the eyes of humans are complex and elegant. As an optical device, the eye can be seen as an optical imaging and detection instrument. The retina of eye acts as a colored high-resolution photosensor. The operation of the two eyes as a pair provides binocular vision that enables one to determine three-dimensional location and distance and the speed of distant objects. The complex structure and relation between the eye, brain, nerves and blood flow provide rapid feedback loops for accommodation and ocular movement to complete the vision function. In this thesis, the binocular vision and nerve brain functions are not considered, and human eye modeling is performed for only the optical and imaging functions of the eye.

To model the human eye, it is necessary to know the optical properties of the eye's elements. These elements are the cornea, iris, crystalline lens, and retina and are shown in Figure 1.1. The cornea is a transparent layer of tissue of approximately 0.55 mm in thickness with refractive index slightly higher than that of water, which, in the visible region is nominally 1.333. The cornea can be seen as the extension of the sclera, the white hard part of eye that forms the oval- shaped object. It is made of the same material of sclera, but with a highly organized orientational arrangement of its

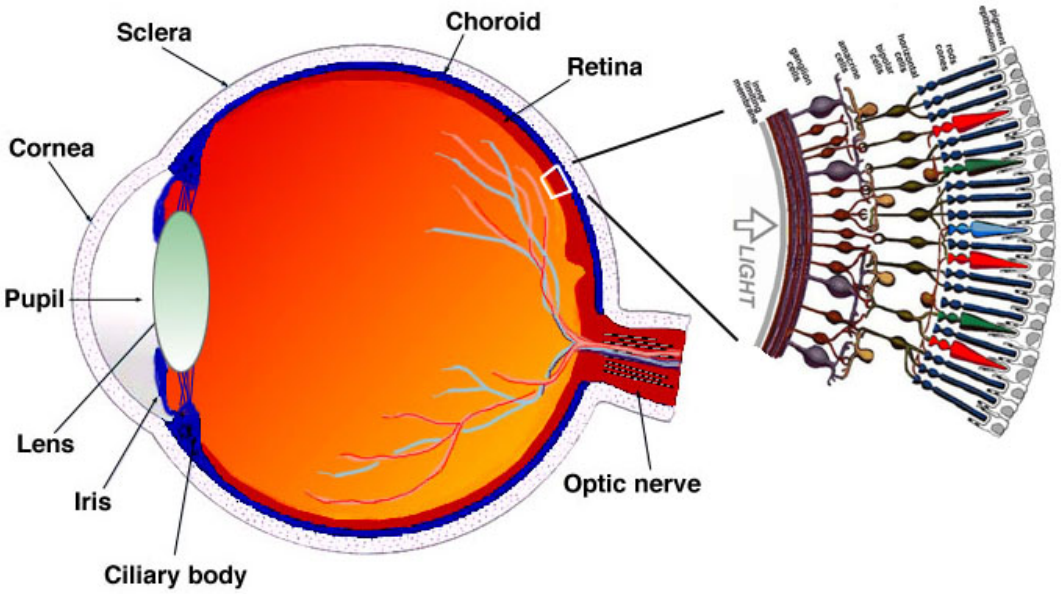

Figure 1.1 Human eye and its optical elements. The upper side in this figure is the tempo side. The lower side is the nasal side.

fiber structure. The cornea provides approximately 2/3 (~ 43 diopters) of total focusing power of eye (~ 57 diopters). Similar to the shutter of a camera, the iris controls the size of pupil and, therefore, the amount of light entering the eye from the environmental illumination. The typical diameter of the pupil is about 1.5 mm in bright light and about *8* mm when it is dilated with drugs. The maximum diameter of pupil in the total darkness reduces with age. The good quality of vision exists only when the pupil is about 2 to 5 mm. When the environment is dark and the pupil diameter is larger than 5 mm, the aberration degrades the imaging quality. If the environment is too bright and the pupil is smaller than 2 mm, the optical diffraction reduces the imaging performance. Only a properly illuminated environment provides optimized visual performance. The crystalline lens is the transparent biconvex structure lying between iris and vitreous humor of the posterior chamber. It consists of a soft outer part, the cortex, and a denser inner part, the nucleus. The accommodation of the eye is the increase in thickness and convexity of the crystalline lens in response to ciliary muscle contraction in order to focus the image of near object onto the retina. The anterior and posterior chambers, which are filled with aqueous humor, a gel-like material, are divided by the lens and iris. The index of refraction of aqueous humor is about 1.336. Located at the far back, the retina works as the film of camera. It consists of the photosensors, the nervous system, and the pigmented part. The optical axis of the eye is different from the visual axis due to the location of the central fovea, the most sensitive area on retina. The fovea is located at about five degrees temporally and two degree upward. To the author's knowledge, all the theoretical anatomic models of human eyes ignore this displacement. The optical parameters of a typical human eye are listed in Table 1.1.

Table 1.1 Optical parameters of typical human eye. R indicates surface radius, t is the distance to next surface, n is the index of refraction between surfaces

Surface Radius	Distance	Refractive Index
R_1 (air to cornea) 7.8 mm	t_1 (cornea) 0.6mm	1.376
R_2 (cornea to aqueous) 6.4 mm	t_2 (aqueous) 3.0mm	1.336
R_3 (aqueous to lens) 10.1 mm	t_3 (lens) 4.0mm	1.386–1.406
R_4 (lens to vitreous) 6.1 mm	t_4 (vitreous) 16.9mm	1.337

Since early 1900, numerous eye models have been developed to study the optical performance of the human eye. Schematic eye models that can reproduce optical properties from anatomy are especially useful. They can be used in the design of ophthalmic or visual optics, to simulate experiments, to predict the effect of refractive surgery or implants, and to understand better the role of the different optical components. The development of schematic eye models will be described using, in chronological order, some of the most popular published eye models:

Gullstrand [A. Gullstrand, 1909]

Published in 1909, this pioneer model was anatomically accurate to the first order and had been adopted universally in optometry text books. It included six spherical surfaces. Four surfaces described the front and back surfaces of the cornea and the lens. The other two surfaces were used to describe the core of the lens with a higher refractive index. The Gullstrand model included two sets of parameters, one for the relaxed-eye condition and the second for the accommodating condition using lens of higher refractive power. This model did not consider the chromatic effect. It was however, sufficient for predicting the quality of imaging of the human eye when the pupil size was not too large, the field angle was sufficiently small, and the spherical aberration value wasn't influential. Decades later, many research groups including the University of California/ San Diego group still constructed eye models based on the Gullstrand parameters.

Le Grand [Villegas ER, 1996]

In 1964, Le Grand proposed a modified Gullstrand model. The essential feature of this modification was the use of wavelength-dependent refractive indices of the cornea, the aqueous humor, the crystalline lens and the vitreous humor. The refractive indices were

assumed to be real and not complex quantities; i.e., no absorptive loss was considered. Using the reported values given by Le Grand (1956), the refractive indices were represented as polynomial functions of the wavelength.

El Hage and Berny [El Hage and Berny, 1973]

Their studies of the crystalline lens showed that it had spherical aberration opposite in sign to that of the cornea, resulting in low ocular spherical error of various amounts. They varied the asphericties of both lens surfaces to match the measurements to all four surfaces.

Kooijman [Aart C. Kooijman, 1983]

Kooijman constructed in 1983 an eye model with spherical and aspheric surfaces and calculated the retinal illumination for Ganzfeld luminance field. The resulting retinal light distribution was nearly homogeneous over the whole retina. (The homogeneity was not significantly influenced by the size of the optical surfaces.) The corresponding retinal area and the luminous flux entering the eye are calculated as functions of the size of the visual field. The values of the length of the light path through the crystalline lens and of the angle of incidence on the retina were described as functions of the angle in the visual field. Kooijman model was a result based on light distribution on the retina from experiment.

Navarro [R. Navarro, 1985]

From this basic model, there have been two major trains of development. On one hand, simplified reduced eyes have been derived. On the other hand, attempts are made to follow anatomy more accurately, incorporating a gradient index (GRIN) crystalline lens, which is sometimes approximated by a shell structure.

In order to harmonize these opposite tendencies Navarro proposed a schematic eye model that offers a trade-off between accuracy and economy (simplicity). The earlier Navarro model, which is constructed based on anatomical data and is designed to reproduce image quality on-axis, has been transformed into a wide angle model, by simply adding a spherical image surface that plays the role of the retina. This model captures the main features of the wide angle optical design of the human eye, with minimum complexity: 4 conic optical surfaces plus a spherical image surface.

Indiana eye model [L. N. Thibos, 1992]

Since the early work of Helmholtz in 1909, the wavelength variation of the ocular focal power had been described using a reduced schematic eye model that consisted of a simple spherical lens with an interior volume of water. The chromatic aberration of the reduced eye was attributed solely to the wavelength variation of the refractive index of water. By including a pupil in the model, the reduced eye also accounted for two forms of transverse chromatic aberration: difference of magnification and difference of position. Calculation of the optical image quality was particularly easy with such a simple physical model, especially if the model's spherical aberration is ignored.

Although the reduced eye accounted well for the major features of ocular chromatic aberration in human eyes, there were at least three areas in which the model required improvements. First, published measurements of the magnitude of chromatic aberration had consistently shown that the model did not fit the data well for the shorter wavelengths of light. Second, the traditional model had a significant amount of spherical aberration, which caused a nonlinear relationship between transverse chromatic aberration and pupil location that was not always evident in the data. Third, more of the

underlying anatomical data, such as the asphericities of the surfaces, the centration of optical and neutral axes of the eye and the gradient structure of the crystalline lens, which supported the model, were needed. To help specify the centration of optical and neural axes of the eye, various reference axes have been defined as shown in the center of Figure 1.2. The optical axis, the visual axis, the fixation axis and the achromatic axis of the eye are specified. Angle α presents the location of the fovea relative to the model's axis of symmetry. Ψ and θ represent the decentration of the pupil relative to the visual axis of maximum neural resolution.

In 1992, about one decade after the work of Kooijman and two decades after that of El Hage and Berny, Thibos at Indiana University introduced the "Chromatic Eye" model. This is a reduced schematic-eye model, as shown at the bottom panel of Figure 1.2, of ocular chromatic aberration that consisted of a pupil and a single, aspheric refracting surface between the air and the chromatically dispersive ocular medium. This model was designed to describe accurately the eye's transverse and longitudinal chromatic aberration while at the same time disregarding spherical aberration effects (at least for the emmetropic wavelength). The basic assumption of this eye model is that the pupil is well centered on the visual axis. This eye model had a refractive index that changed more rapidly with the wavelength than did water. This optical design was achieved by employing an elliptical refracting surface which had zero spherical aberration, the so-called Cartesian oval. The resulting chromatic-eye model provided an improved account of both the longitudinal and transverse forms of ocular chromatic aberration. All dimensions are in millimeters. Circles mark the location of the nodal point (N), center of retinal sphere (C), center of exit pupil (E'), anterior focal point (F), and

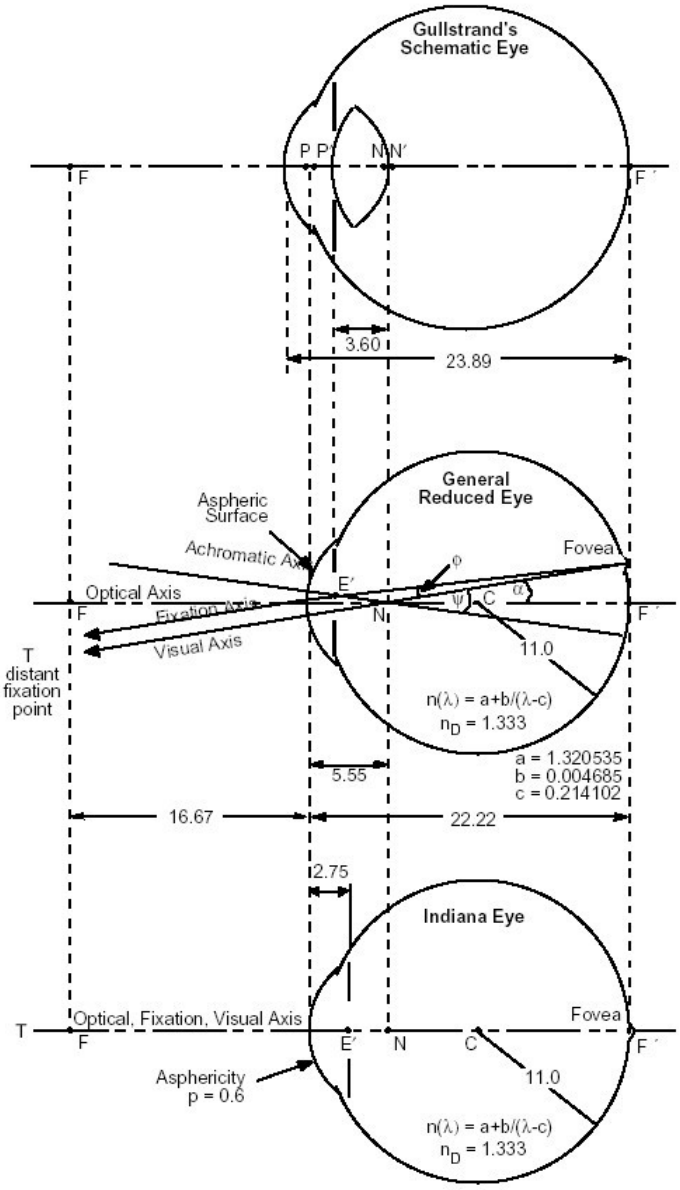

Figure 1.2 Comparison of anatomic based eye model (upper) and reduced eye model (middle and lower).

posterior focal point (F') of the reduced eye. Surface of the reduced eye is located midway between the principal points P, P' of the Gullstrand model.

Arizona [John E. Greivenkamp, 1995]

A research group in the University of Arizona developed several years later a methodology to predict changes in visual performance that result from changes in the optical properties of the eye. In this method, optical ray-tracing of schematic eyes was used to calculate the point spread function (PSF) and the modulation transfer function (MTF) of the visual system. The Stiles-Crawford effect, photopic response, diffraction, and the retinal contrast sensitivity are included in the model.

Liou [Hwey-Lan Liou 1997]

The objectives of Liou and Brennan were to develop a schematic eye model that can be used over a broad range of applications, such as the prediction of the result of refractive surgical procedures, the design of contact lens and spectacles, and near vision accuracy. In 1997 the authors proposed a model eye that consisted of four aspheric refracting surfaces and a gradient-index lens and whose anatomical, biometric, and optical parameters bore close resemblance to reality. This sophisticated model eye provides spherical aberration values within the limits of empirical results and predicts chromatic aberration for wavelengths between 380 and 750 nm. It provided a model for calculating optical transfer functions and predicting optical performance of the eye. However, the use of gradient-index lens increases calculation time dramatically when performing complex ray tracing analysis.

University of California San Diego [Zhu L 1998]

For the study of human eye aberrations and their compensation to achieve high-resolution retinal imaging, the UCSD group introduced a mathematical eye model using Gullstrand's six-surface eye model that was modified by clinically measured aspherical data. Ray tracing was used to characterize aberrations and point spread functions of the eye model. By using the Zernike polynomial decomposition of the calculated pupil function, they quantified the wave-front aberrations. Based on calculated PSFs, they designed optical inverse filters to reduce the aberrations for a large pupil size and to improve the resolution. Spherical aberration and oblique astigmatism were found to be in good agreement with published experimental measurements.

Popiolek [Popiolek-Masajada, 1999]

In 1999, Popiolek presented a human eye model with a new gradient index crystalline lens. The crystalline lens shape at different accommodation levels was described by a single function which was a combination of hyperbolic cosine functions and hyperbolic tangent functions. Using the experimental data published in the literature, a model of the variation of the external lens shape with accommodation was created. Analytic results for the lens shape parameters and gradient index distribution for different accommodation levels were given.

For comparison, the optical parameters of many published eye models are provided in Table 1.2.

To our knowledge, all the published eye models today are constructed to describe normal 20/20 eye condition without pathology. The parameters adopted in these eye models are typical (or average) numbers of healthy eyes of young adults. There is no

Table 1.2 indicates the parameters of some important eye models.

parameter	authors:		surface: cornea front	cornea back	pupil (stop)	anterior lens	posterior lens	Retina
Radius (mm)	Gullstrand 1909		7.7	6.8	Infinity	10.0 / 7.911core	-5.76 core / -6.0	-11.5
	Navarro 1999		7.72	6.5	Infinity	10.2	-6	-12
	Liou 1997		7.77	6.4	Infinity	12.4	-8.1	-12
	AZ 1995		7.8	6.5	Infinity	11.03	-5.72	-12
	Popiolek 1999		7.77	6.4	Infinity	13	-8.9	-12
	UC San Diego 1998		7.7	6.8	Infinity	10.0 / 7.911core	-5.76 core / -6.0	-12.5
	Kooijman (Netherland) 1983		7.8	6.5	Infinity	10.2	-6	-10.8, -14.1
Conic Constant	Gullstrand		0	0	0	0	0	0
	Navarro		-0.26	0	0	-3.1316	-1	0
	Liou		-0.18	-0.6	0	-0.94	0.96	0
	AZ		-0.25	-0.25	0	-4.3	-1.17	0
	Popiolek		-0.19	-0.8	0	defined	defined	0
	UC San Diego		-0.26	0	0	-3.1316	-1.0081	0
	Kooijman (Netherland)		0 or -0.25	0	0	0 or -3.06	0 or -1	0
Thickness (mm)	Gullstrand		0.5	3.1	0	3.59	16.8	-
	Navarro		0.55	3.05	0	4	16.3203	-
	Liou		0.5	3.16	0	4.02	16.27	-
	AZ		0.55	3.05	0	4	16.6	-
	Popiolek		0.51	3.71	0	3.71	16.07	-
	UC San Diego		0.5	3.1	0	3.6	17.1854	-
	Kooijman (Netherland)		0.55	3.05	0	4	16.6	-
medium			**Cornea**	**Aqueous**	**Aqueous**	**Lens**	**Vitreous**	**Retina**
Wavelength -dependent Index of Refraction	Gullstrand	wavelength independent	1.376	1.336	1.336	1.385 shell 1.406 core	1.336	-
	Navarro	458 nm	1.3828	1.3445	1.3445	1.4292	1.3428	-
		543 nm	1.3777	1.3391	1.3391	1.4222	1.3377	-
		589.3 nm	1.376	1.3374	1.3374	1.42	1.336	-
		632.8 nm	1.3747	1.336	1.336	1.4183	1.3347	-
	Liou	Index, n_d	1.37487	1.3349	1.3349	Gradient	1.334905	-
		Abbe, V_d	61.661184	55.08224	55.08224	1.368 ~ 1.407	55.101116	-
		D_{pgf}	0.29441	0.29441	0.29441		0.295752	-
	AZ	Index, n_d	1.3771	1.3374	1.3374	1.42	1.336	-
		Abbe, V_d	57.136364	61.345455	61.345455	41.727273	61.090909	-
		D_{pgf}	0.30303	0.309091	0.309091	0.295455	0.309091	-
	Popiolek	wavelength independent	1.3767	1.336	1.336	1.461	1.336	-
	UC San Diego	wavelength independent	1.376	1.336	1.336	1.386 shell 1.406 core	1.336	-
	Kooijman (Netherland)	wavelength independent	1.3771	1.3374	1.3374	1.42	1.336	-

n_d: index of refraction at sodium d-line, 587.5618 nm, **V_d**: Abbe number, **D_{pgf}**: partial dispersion number.

specific gender, age, or race characteristics associated with any of these models. Further, there is no eye model established to describe variation in population. The only eye models with refractive errors (or ametropia) are Thibos' model [Thibos (1992)] where the axial length of this simplified eye model was varied and Chen's model [Chen (2000)] where an intraocular power was introduced. Both models simulate refractive error with only one single variable. The objective of this thesis is to construct a model of this most common vision disorder– ametropia, or, in more comprehensible words, near- and far-sightedness. To achieve the goal, a normal 20/20 eye model must first be in hand. Variables that could cause this disorder should then be introduced into the normal eye model to simulate various refractive statuses. Previously, comparisons were made for the photorefractive (PR) images (Ying-Ling Chen, 2000 & 2003) using several models, including the Gullstrand model [A. Gullstrand, 1909], the Australia Liou model [H-L. Liou, 1997], Navarro's model [Isabel Escudero-Sanz, 1999], and UC San Diego model [Zhu L 1998]. Based on their applications, many published eye models that emphasize accurate paraxial performance and ignore the individual difference in aberrations are not suitable for a wide range of application including the evaluation of ocular instrument that often work with a large pupil and wide angle of field. Therefore, in the subsequent chapter, a general ametropic model is constructed based on parameters of the Navarro *20/20* eye model, which was developed with regard to off-axis aberrations for a field angle up to *60* degrees. After the general ametropic model is constructed, the optical performance of this eye model is evaluated and compared to measured data from published papers in chapter 3. The last chapter concludes the ametropic eye modeling work.

Chapter 2

Simulation of ametropic human eye

The most general cause for the poor optical performance of the naked eye in the population is the refractive error. For an emmetropic eye, or normal 20/20 eye, with fully relaxed accommodation the image of distant objects would be sharply focused on the retina surface. For an, eye with refractive errors, ametropia is the condition in which with the eye at rest (without accommodation effort) light rays from the distant objects are not in conjugate focus with the retina. In other words, although the image of a distant object is focused by the ametropic eye into a sharp image, this image falls on either the front (near-sighted or myopic condition) or the back (far-sighted or hyperopic condition) of the retina instead of onto the retina surface (see Figure 2.1 (b) and (c)). Based on how the image is defocused, ametropia is distinguished as different types. When this defocus is rotationally symmetric in an eye, the refractive error is called spherical. If the defocus is not symmetric and can be described by the maximum and minimum defocus lying on two perpendicular meridians, the power difference of the two defocus points is called the cylindrical refractive error, which is the condition of regular astigmatism (see Figure 2.1 (d)). Astigmatism is caused by one or more of the optical surfaces of the eye being toroidal, tilted, or displaced from the axis. Spherical, cylindrical (error), and axis of

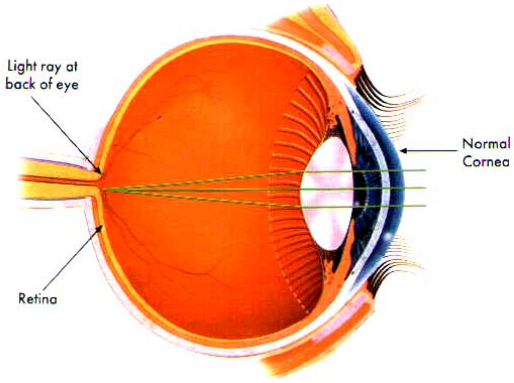

(a) Normal eye

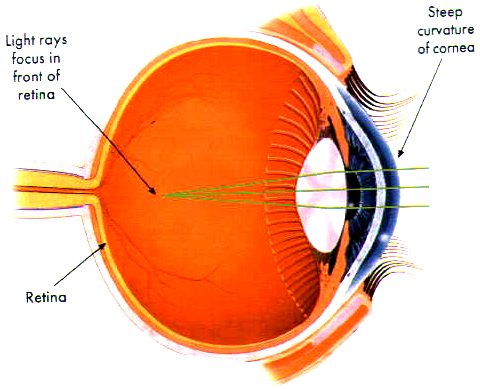

(b) Myopic (near-sighted) eye

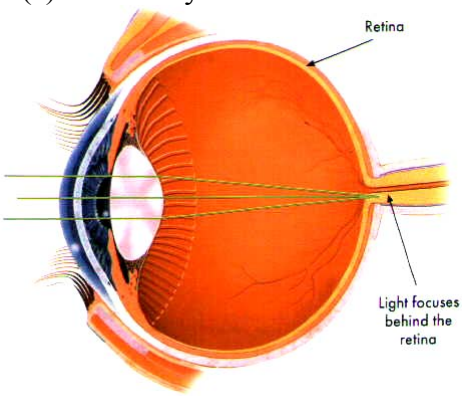

(c) Hyperopic (far-sighted) eye

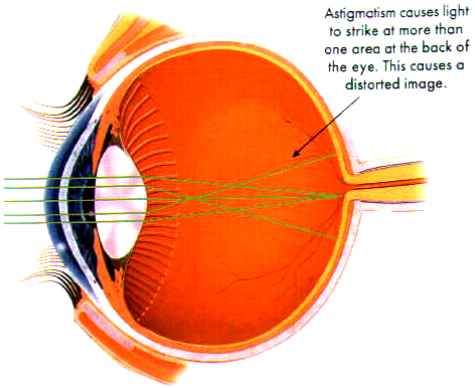

(d) Astigmatism

(e)

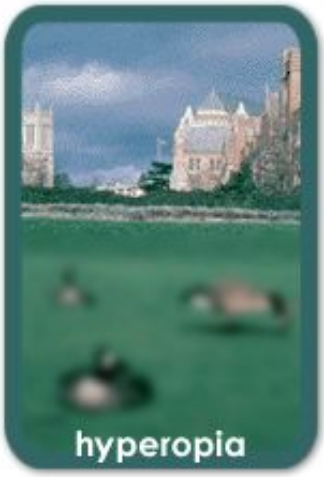

(f)

(g)

Figure 2.1 The focus of parallel pencil rays from a distant object in (a) normal and (b)-(d) ametropic eyes (e)-(g) the vision of ametropic eyes

defocus are normally given to patients after a visual acuity examination in (*S, C, X*) form. All of above refractive errors are normally corrected with eye glasses, contact lens, or laser cornea surgery.

In the followed sections, the literature of the prevalence of ametropia is reviewed. The computer simulation of axial, refractive, and index ametropic eye models is described next. Before the end of this chapter, the three simplified models are compared to the published experimental data, and a general ametropic eye model is constructed and proposed for the first time.

2-1. Distribution of ametropia: age, gender, and race

Before modeling human eyes, we must bear in mind that the human eye conditions vary al least with age, gender, race, environmental condition, sickness, and medication. Even for an individual, the eye condition varies during a day. A computer simulated model eye represents a typical condition of human eyes that is not likely to be found anywhere in the world. However, eye modeling provides a reference where the small variations in population can be modulated and the effect and performance can be evaluated.

The average refractive error in population varies with age. The results from three age-related studies were reproduced in Figure 2.2. Though the data acquired in by Saunder in 1986 [Saunter, 1986] differed from the result taken by Slataper in 1950 [Slataper 1950], both showed the hyperopic (farsighted) nature in children and the degree of positive refractive error reduced monotonically with age until about 20-30-year old when the growth came to a halt. Following a stable stage of about 20 years, the vision

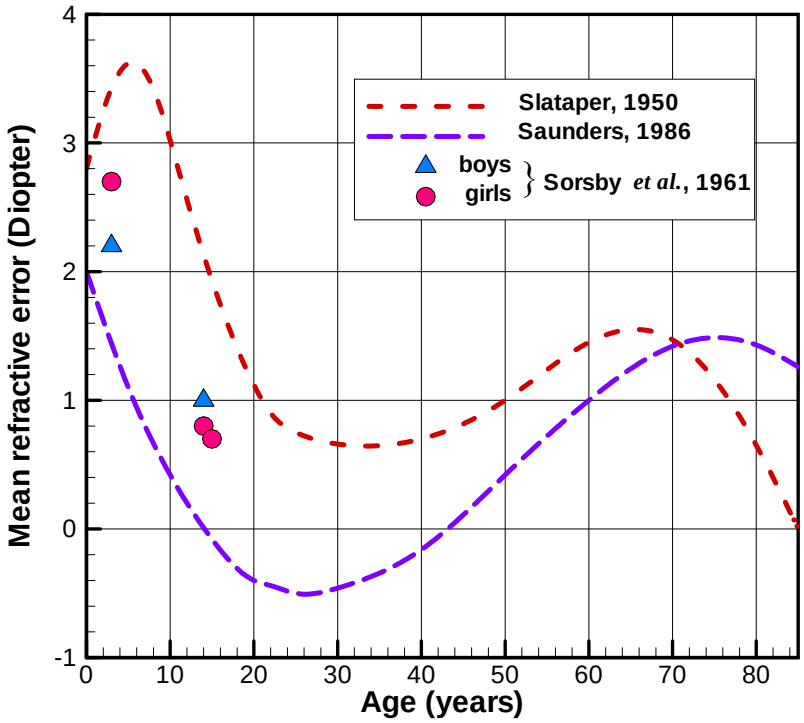

Figure 2.2. Age dependence of mean refractive error. [Slataper, 1950, Saunders, 1986 and Sorsby 1961]

gradually tended to far-sightedness again. The train of events in the 0-20 years period was related to the growth of eye ball. From the study of Sorsby in 1961, the axial length and radius of cornea curvature increased and the power of lens decreased with the growth [Sorsby 1961]. His results of some 3-, 14- and 15-year old boys and girls were also plotted in triangle and circle symbols in Figure 2.2 for comparison.

According to the study by Farrell and Booth in 1984 [Farrell, 1984], the age-dependent prevalence rate of corrective lens wear was given in Figure 2.3. The study showed the need of using corrective lens increased monotonically with age and females had ~ 5-10 % higher prevalence rate over males throughout. Comparing Figure 2.2 and 2.3, it is notable that the need of wearing corrective lens does not directly relate to the refractive errors. For age older than 40 years, the reduction of accommodation capability played a major role.

Figure 2.4 was the age, gender, and race dependence of refractive-error prevalence rate in 50 years and older population in the U.S. released by National Eye Institute (NEI) in 2002. As shown in the two figures, the near-sightedness prevalence rates reduced (upper figure) while the far-sightedness prevalence rate increased (lower figure) with age for all races and both genders. This feature agreed with the two studies in Figure 2.2. The white population seemed to have highest and the black to have the lowest prevalence rates compared to other races. Females in all races had higher prevalence rate in hyperopia > + 3 diopters than males. In myopia worse than -1 diopter, white and black females had higher prevalence rates before 70-years of age.

For young Caucasian adults, the distribution functions of refractive errors were reported from many cross section studies, and some of the results were reproduced and

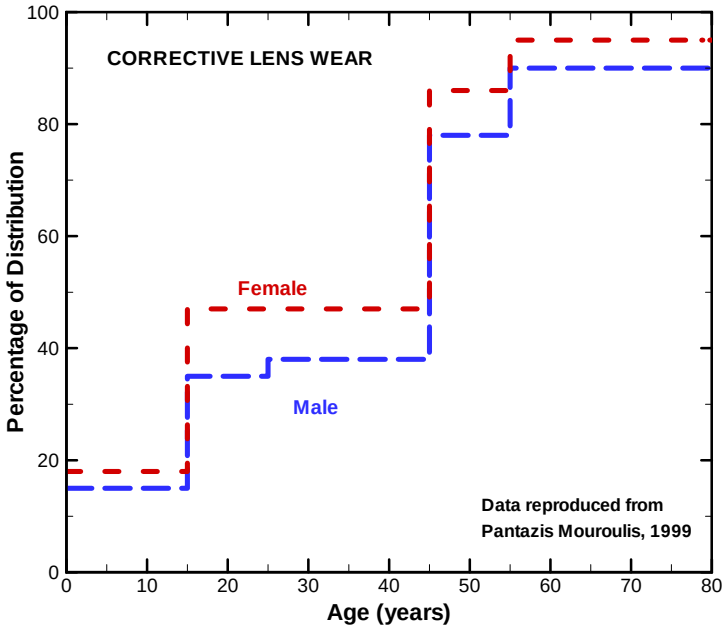

Figure 2.3. Age dependence of prevalence percentage in female and male wearing corrective lens.

[Farrell, 1984]

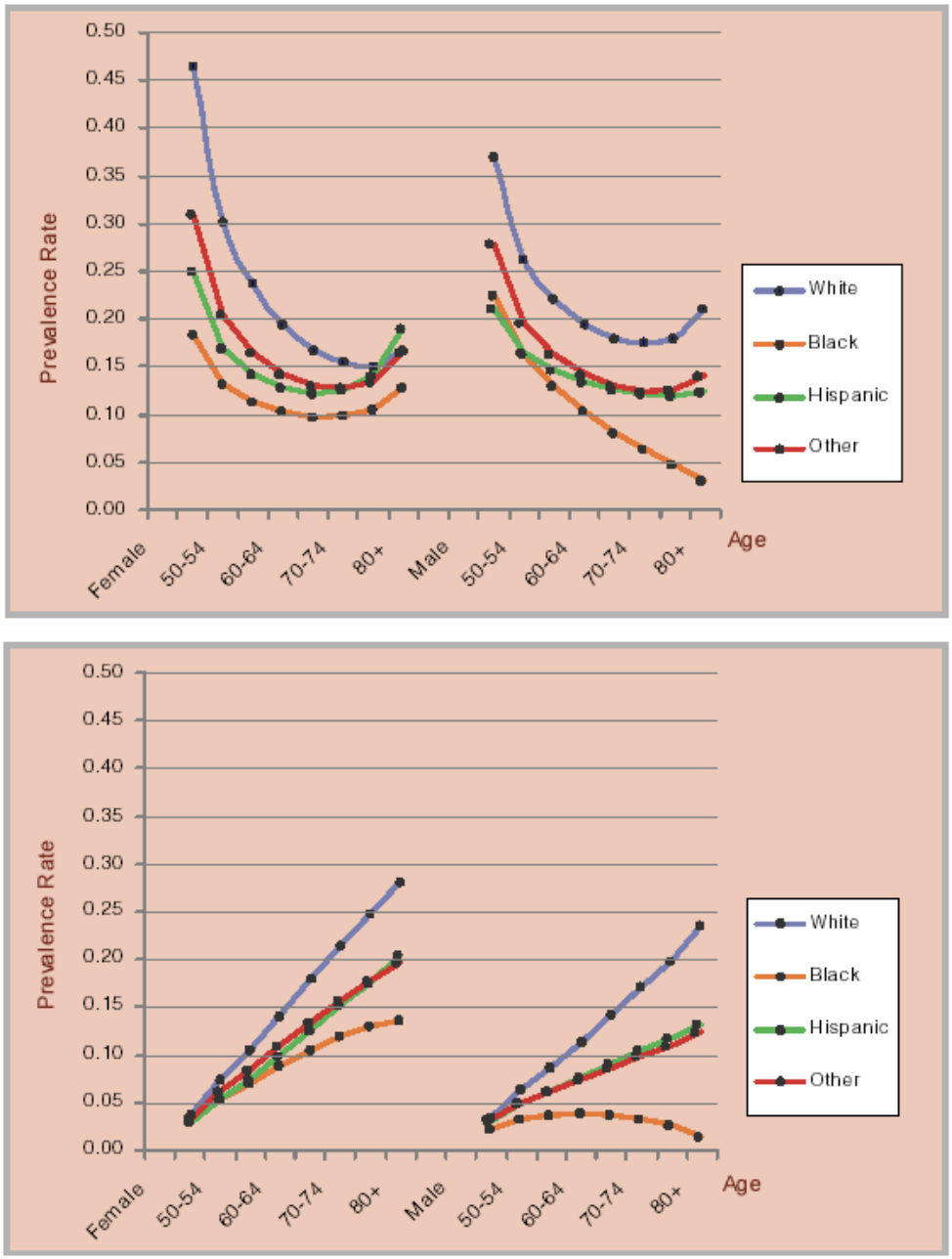

Figure 2.4 Age, gender, and race dependence of refractive error in 50 years and older population in the US. Upper: myopia < -1 diopter, Lower: hyperopia > +3 diopters. [John A. Shoemaker, 2002]

presented in Figure 2.5. All three results of males in Figure 2.5 showed more than 70 % of the young adult population had emmetropic or mild hyperopic condition less than +2 diopters, which could be easily compensated with accommodation. In Stenstrom's study, again, females tended to have worse refractive condition in comparison to males.

Figure 2.6 showed a study of cylindrical refractive error for adult population performed in 1971 [Lyle, 1971]. The figure included 96% of cases in which the most powerful meridian were within 30° of the horizontal (against the rule) and within 30° of the vertical (with the rule). The distribution function showed greater than 70% of population had a cylindrical error less than 1 diopter and did not require the cylindrical correction.

2-2. Ametropia cause factors and computer modeling

Following the brief description of refractive errors in the beginning of this chapter, one could think of many possible causes that may contribute to this visual disorder. The names of axial ametropia and refractive ametropia are given in most of optometry text books to identify refractive errors from their causes. The axial ametropia is a result from the shortening or lengthening of eye ball on the optical axis. The refractive ametropia results from either the curvature variation of the ocular elements or refractive index variations of lens. There is no clear statistical data that support and describe the correlation of these cause factors and their distribution. In this thesis, using a commercial optical computer code, ZemaxTM (ZEMAX Development Corporation, San Diego, CA, USA), investigation is applied to causal factors of axial length, cornea curvature, and refractive index gradient As mentioned at the end of the previous chapter, many newly

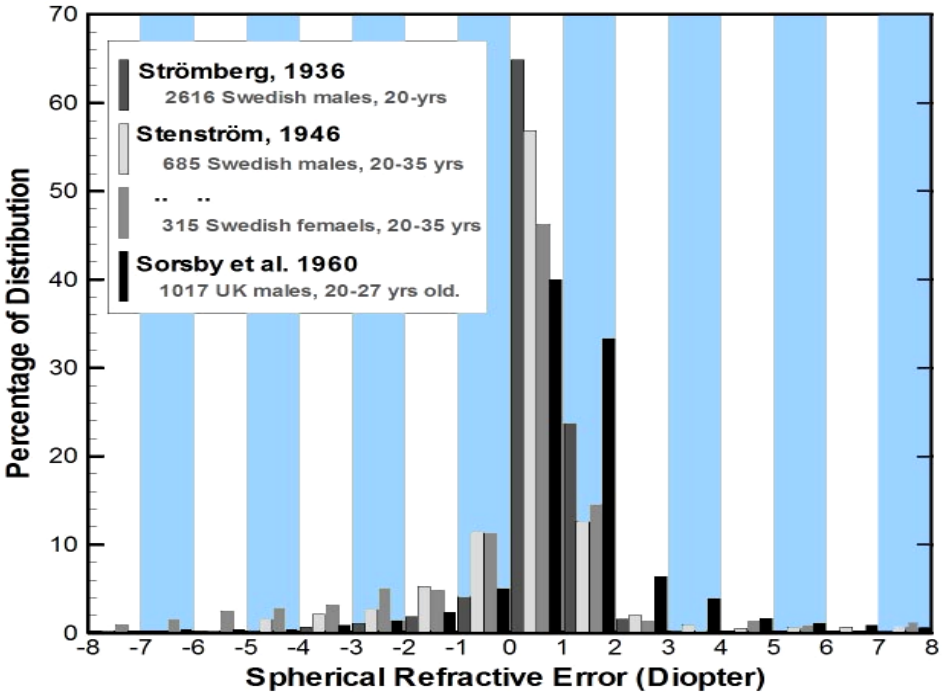

Figure 2.5 Percentage distribution function of refractive error in population. [Strömberg, 1936, Stenström, 1946 and Sorsby, 1960]

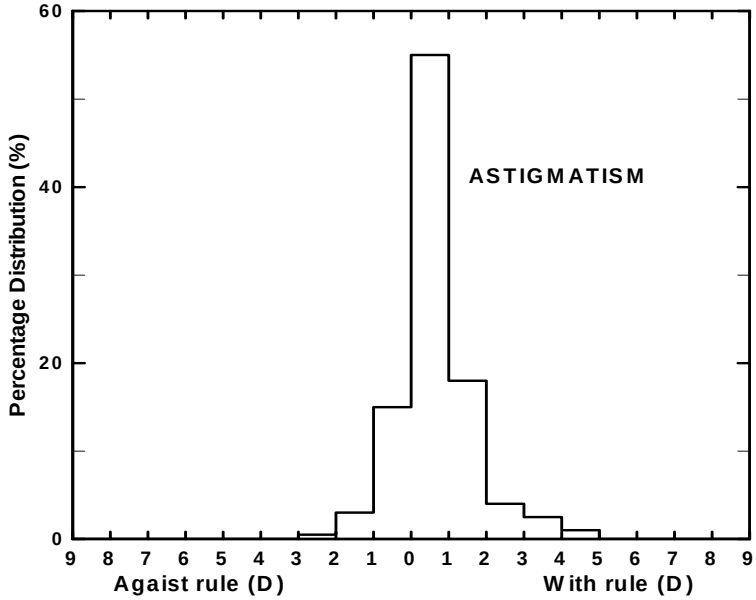

Figure 2.6 Distribution of cylindrical refractive error [after Lyle, 1971]

published eye models are evaluated using the computer code and as a result, the parameters of Navarro eye model are adopted for emmetropic eye model in this research. The optical parameters of Navarro model are listed in Table 1.2. The chromatic aberration, spherical and astigmatism aberrations of this reconstructed model eye are calculated and compared to the original published paper [Isabel Escudero-Sanz, 1999] to ensure the accuracy of the modeling.

To investigate the relationship of the causal factors, the pure axial ametropic eye is synthesized by varying only the posterior axial length (model A); the pure index ametropic eye by varying only the variable of virtual power of near pupil and lens position (model B); and the pure refractive ametropic eye by varying only the variable of surface curvature (model C). The three ametropic eye models are described below:

Model A --- the pure axial ametropic eye model: The only adjustable parameter in this modeling is the vitreous body thickness on the posterior chamber. During the computation, this variable is iteratively varied from emmetropic condition until the corresponding far point position reaches the desired refractive error. All the far point distances are determined under paraxial eye condition. The reason is that the Navarro model eye is emmetropic only under the paraxial condition. With a larger pupil diameter, the far point of the Navarro model eye will not occur at infinity due to the effect of aberrations. As an example, for a 3-mm-pupil Navarro eye, there is a small refractive error of 0.18 diopter. Therefore, in all of our studies using the Navarro model as the emmetropic standard, the refractive status of a model eye is always determined under the paraxial condition.

Also obtained in the calculation are the results with different asphericity, the degree of peripheral flattening of the front cornea surface. The conic constant, Q, which is used to describe the asphericity of optical surface, is originally -0.26 in the Navarro model. It is the only parameter used in almost all of today's eye models (see Table 1.2) to produce the aspheric property and difference from spherical surfaces of eye elements. Unless additional parameters or user-defined surface are introduced in the computer modeling, the conic constant in each surface of cornea and lens is the only index that determines aberration degree of the eye. Up to this date, all the eye models are azimuthally symmetric. To the author's knowledge, the conic constant varies significantly from one person to another. Even for an individual, the Q number is generally different in the four angular quarters temporal, nasal, upper and lower of the eyes. From the spherical aberration measurement, the Q number tends to be near -1.0 for infants and toddlers and tends to increase with age.

As shown in Figure 2.8, the deviation of cornea surface from Q = 0 (red symbols on top) to Q = -1.0 (violet symbols at bottom) is observable only near the periphery of cornea. Surprisingly, this 'small' deviation results in a significant difference in the spherical aberration of the eye, and therefore, up to several diopters in the performance of vision in a darkened environment. The resulting curves in Figure 2.7 for different Q numbers are indistinguishable. Since the paraxial condition is assumed for visual refractive error determination, this result is expected.

The conic constant will be further discussed subsequently.

Model B --- pure curvature ametropic eye model: The radius of anterior cornea surface is the only variable to synthesize refractive error. Curvature variations in other surfaces in

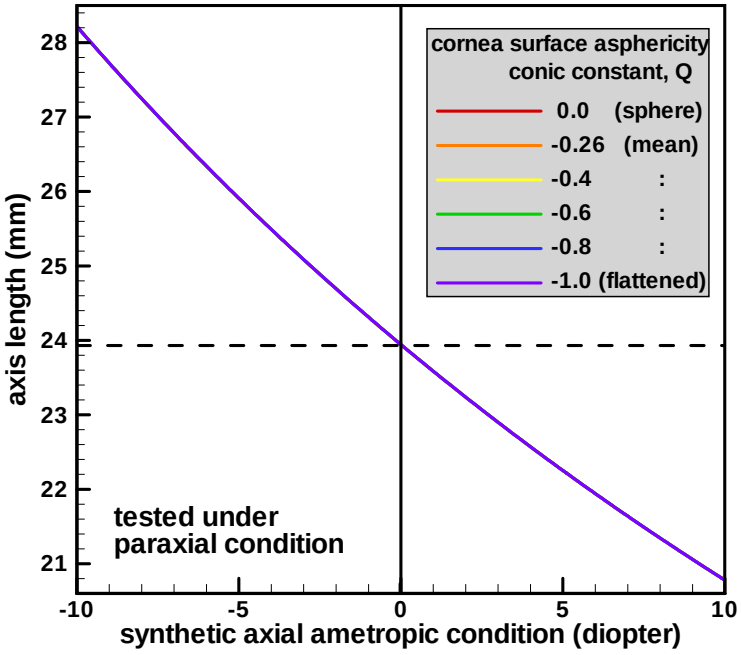

Figure 2.7 Simulation result of pure axial ametropic eye.

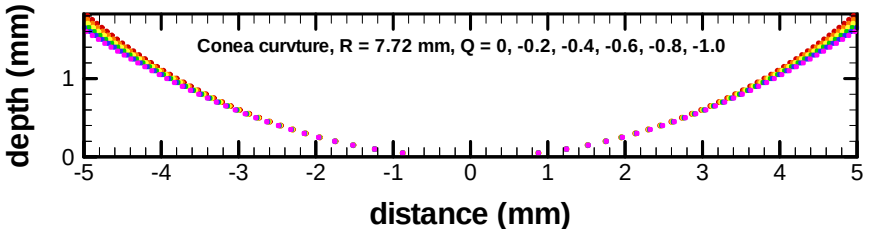

Figure 2.8 Shape of simulated cornea surface over a 10-mm diameter range. The radius of the surface is 7.72 mm. The red symbols represent the spherical surface, Q=0. The orange, yellow, green, blue, violet symbols represent surfaces with Q=-0.26, -0.4, -0.8, and -1.0.

the ocular system were omitted because they provide very small refractive influence compared to the front cornea surface. This is an expected conclusion since the cornea front surface alone is known to provide more than two thirds of the focusing power of the eye. With the single variable of curvature of the first surface of eye, the refractive ametropic eye is obtained, and the result is shown in Figure 2.9.

Model C --- pure refractive index ametropic eye model: The single adjustable parameter in this model is an ideal virtual thin lens with a uniform power introduced at the plane of pupil. Similar to the process in Model A, the power of virtual thin lens is used to be the only variable to approach the desired conjugate point of the retina and obtain the corresponding far point and ametropic condition. The required power of virtual lens for simulating ametropic condition is shown in Figure 2.10. Again, the asphericity of cornea surface does not affect the result.

The three types of specific models are constructed. However, it is not convincing that a severe ametropic human eye is a result of one of the three factors alone. There must be correlations between the causal factors that can be used to construct a more general ametropic eye model. For instance, while the axial length increases, the size of eye ball increases accordingly. It is not reasonable to assume the radius of cornea will remain constant. The task of searching for the correlations will be described in the followed section.

2-3. The general ametropic eye model

In searching for the correlations among the cause-factors of ametropia, experiment data from human subjects is essential. Two published papers from Niall C. Strang 1998

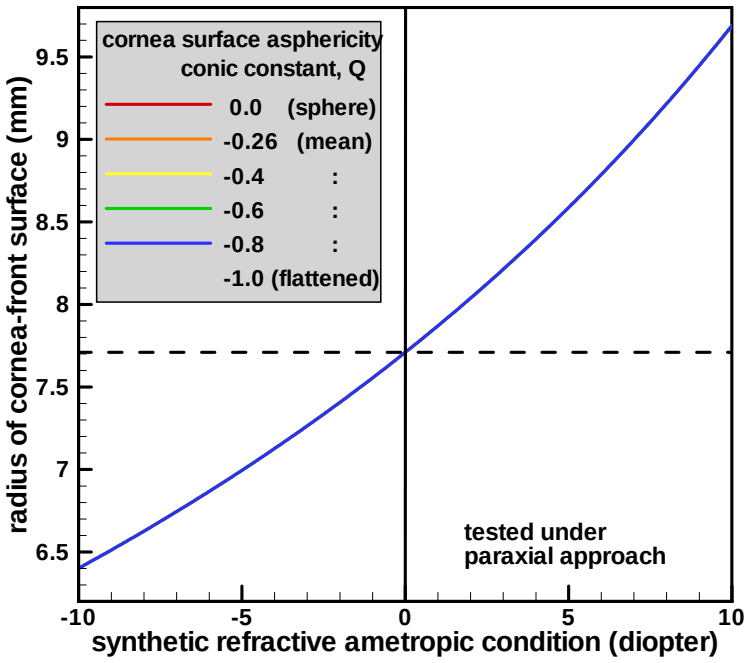

Figure 2.9 Simulation result of pure refractive ametropia.

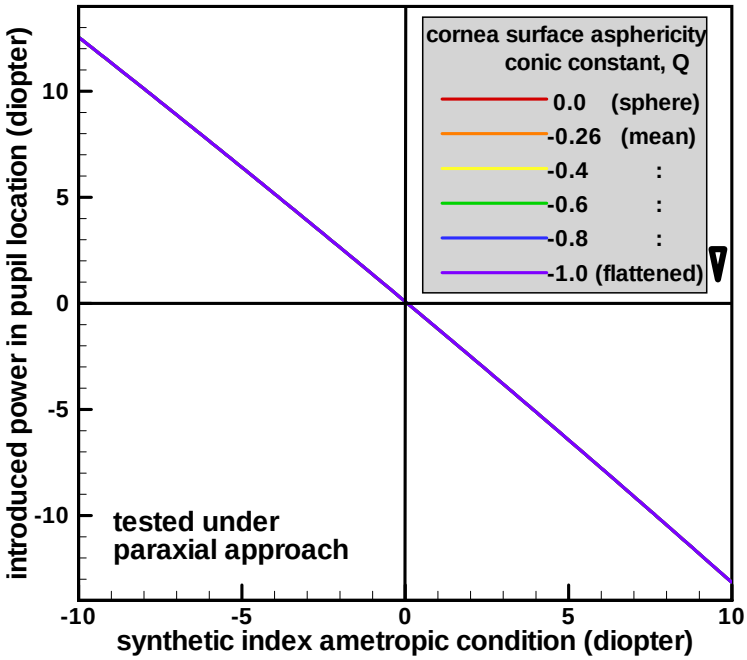

Figure 2.10 Simulation result of pure index ametropia.

[Strang (1998)] and Mainstone JC 1998 [Mainstone (1998)] provide experiment data of axial length and cornea curvatures of human eyes measured in vivo.

In Strang‘s study, 34 young adults with refractive errors ranging from plano (Characterized by no refractive error) to -14 D participated. Axial length and corneal radii were measured on all subjects using an A-Scan Ultrasonography and Allergan Humphrey Auto-Keratometer respectively. All subjects had <0.75 D of astigmatism and were optimally corrected with the appropriate sphero-cylindrical correction with either contact lens or spectacles. The spectacle prescription was measured at a back vertex distance of 15 mm. Soft contact lens were used in all of the subjects with fitting carried out at least 30 min prior to visual acuity measurement. Any residual astigmatic error (B 0.75 D) was corrected with a trial spectacle lens. Visual acuity was measured following both spectacle lens and contact lens correction using two different logMAR Bailey–Lovie high contrast letter charts, each employing an interpolated scoring technique. This method improves the accuracy of VA measurement and thus aids the distinction between subjects with similar VAs. The Bailey–Lovie charts were maintained throughout the study at a luminance of ≈160 cdm^{-2}.

In Mainstone’s measurement, thirty-five subjects, 18 males and 17 females, were selected for the study. Of the 35 subjects, 10 were emmetropic (mean spherical equivalent refractive error, $SE = +0.21 \pm 0.26$ D, range -0.37 to +0.50 D) and 25 were hyperopic (mean $SE = +2.74 \pm 1.72$ D, range +0.62 to +6.00 D). Subjects were recruited from either the student/staff population at the Queensland University of Technology School of Optometry or from the patient database at the QUT Optometry Clinic. All

subjects satisfied the criteria: no anterior ocular pathology, best spectacle corrected distance Snellen acuity of 6/6 or better in the eye to be examined and a cylindrical refractive correction of no greater than -1.50 D. Rigid contact lens wearers were excluded from the study, but soft contact lens wearers were permitted to participate, provided that lenses were not worn on the day of testing. Measurements were made on only one eye of each subject. Central corneal radius of curvature was assessed first using a Bausch and Lomb keratometer (Bausch and Lomb, Rochester, NY). Three consecutive measurements were made, with values for the horizontal and vertical meridians being recorded. One drop of 0.5 per cent cyclopentolate was then instilled. Corneal topography was measured using a computerised videokeratoscope. Four video images of the cornea were captured for each subject, with the best image selected for data analysis. The surface asymmetry index (SAI) was calculated by summing the differences in corneal power between pairs of corresponding points on the corneal surface, each 180 degrees apart, over 128 equally-spaced meridians. A central weighting is given to this value. The surface regularity index (SRI) indicates the regularity of the cornea within a zone delineated by the entrance pupil under standard lighting conditions. In this study, videokeratoscopic image quality was determined by analyzing the SAI and SRI values, with the image displaying the lowest values being chosen for later analysis for each subject. If, for any subject, more than one image had low SAI and SRI values, the image with the greatest corneal coverage was chosen. In cases where videokeratographic image quality was poor for all four images, as a result of unexpected blinking or tear break-up, a second set of four images was captured and analyzed. Thirty minutes after the instillation of cyclopentolate, or when the subject's amplitude of accommodation had decreased to less than two dioptres, subjective

refraction was performed. Following this, one drop of 0.4 per cent benoxinate was instilled into the test eye and three readings of axial length were taken using a BIOPEN hand-held biometric ruler (BIORAD, Glendale, CA). Keratometry and axial length data were averaged to give a single value of each parameter for each subject.

The geometric properties and refractive error of the 69 subjects in these two studies are reorganized and listed in Table 2.1.

In Figure 2.11, the axial length of eyes versus refractive error of the two groups of data is illustrated. A polynomial fitted curve of the combined data is shown in red solid line and the pink band around the fitted curve represents 50% of the distribution. The predicted curve of pure axial ametropic eye model from Figure 2.7 is plotted in black dashed line the same figure for comparison. The comparison shows a close agreement in the myopic region and the two lines deviate when approaching hyperopic region. This result suggests the strong dependence of axial length on refractive error of human eye.

In Figure 2.12, the relation between curvature of cornea front surface and refractive errors of the measured data is shown. As in Figure 2.11, the two groups of data are plotted in square and triangle symbols to be identified and a linear fitting and its 50% distribution are presented in red solid line and pink band. The comparison of pure curvature ametropic eye model (Model B as in Figure 2.9) is also illustrated in the figure in black dashed line. It is apparent that the pure refractive ametropic eye model does not predict the measured curvature dependence on ametropic condition at all. However, if the axial-length-dependence relation (the red fitted curve in Figure 2.11) is adopted into an axial-corrected ametropic eye model and use the cornea surface curvature to compensate the remanding refractive error difference, the curvature vs. refractive error relation would

Table 2.1 The combined data of eyes' axial length and cornea curvature, against the refractive error from the human subjects (Niall C. Strang 1998 and Mainstone JC 1998)

refractive error(D)	axial length(mm)	corneal radius(mm)
0	23.75	7.4
0.2	23.5	7.58
0.2	23.65	7.63
0.3	23.3	7.82
0.4	22.9	7.43
0.4	23.1	7.55
0.4	23.55	7.74
0.4	24.3	7.82
0.5	22.3	7.49
0.7	23	7.59
0.7	23.5	7.66
0.8	22.7	7.42
0.8	23.45	7.54
0.9	22.6	7.48
1.0	23	7.48
1.1	22.4	7.37
1.1	23.5	7.74
1.3	25	8.31
2.3	22.8	7.65
2.3	23.25	7.86
2.5	21.6	7.34
2.6	22.4	7.61
2.8	21.4	7.34
3.4	22.6	7.93
3.5	21.9	7.58
3.5	22.5	7.87
3.7	22	7.54
3.7	22.65	7.89
4.2	22	7.38
4.5	22.2	7.56
4.5	23.2	8.18
5.5	20.75	7.33
5.9	20.75	7.68
6.0	21.1	8.02

refractive error(D)	axial length(mm)	corneal radius(mm)
-0.4	23.8	7.51
-13.8	28.84	7.43
-11.1	27.5	7.71
-10.8	28.9	7.98
-9.8	29.9	8.3
-10.0	28.4	7.99
-8.8	27.9	7.63
-8.8	27.5	7.68
-8.6	29.8	8.23
-8.6	27	7.53
-8.45	27.1	7.52
-7.6	25.8	7.84
-6.7	24.8	7.9
-6.5	26	7.81
-6.0	24.8	7.95
-6.3	27.7	7.61
-5.6	26.8	7.42
-5.5	26	7.51
-5.5	25.9	7.9
-5.5	25.15	7.98
-5.3	25.45	7.81
-5.3	25.35	7.96
-5.0	25.1	7.57
-4.3	25.1	7.46
-4.3	25.55	7.82
-3.5	25.4	7.9
-3.5	24.6	7.94
-3.0	26.45	7.61
-2.5	24.4	7.87
-2.3	24.27	7.8
-1.9	24.5	7.52
-2.0	23.22	7.61
-0.4	23.7	7.9

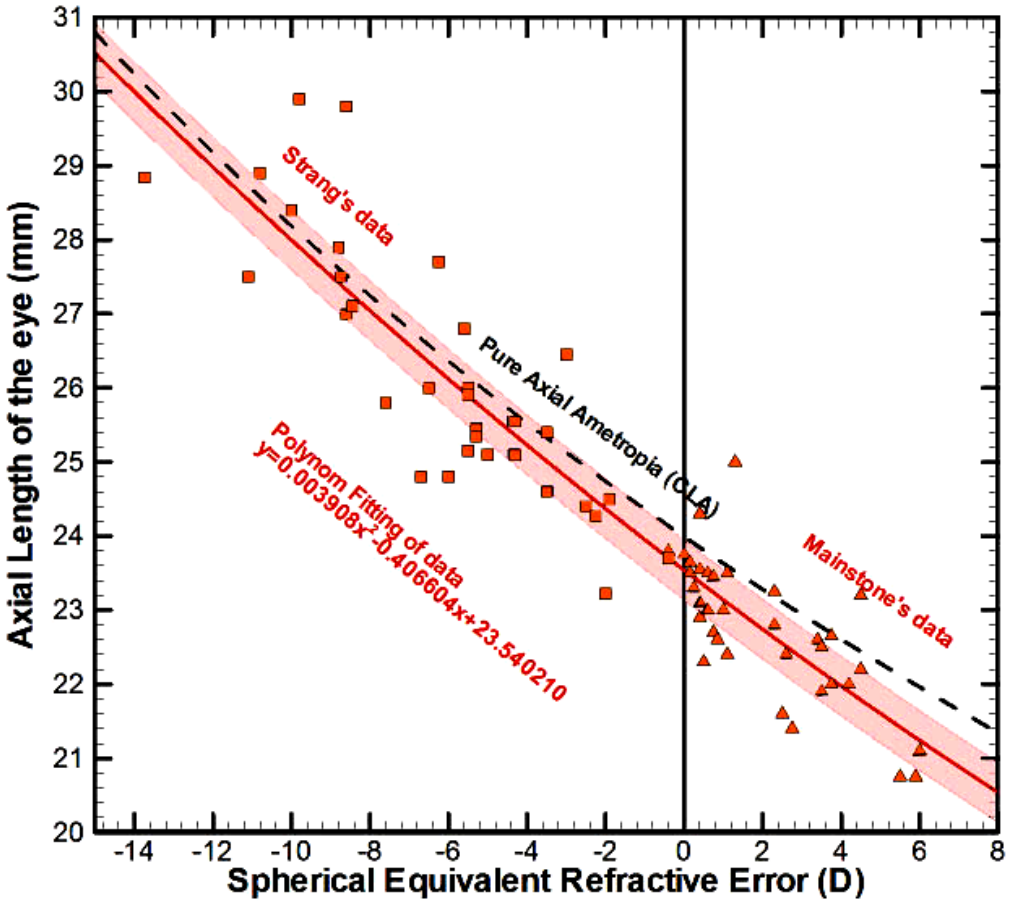

Figure 2.11 Axial length of eye vs. refractive error.

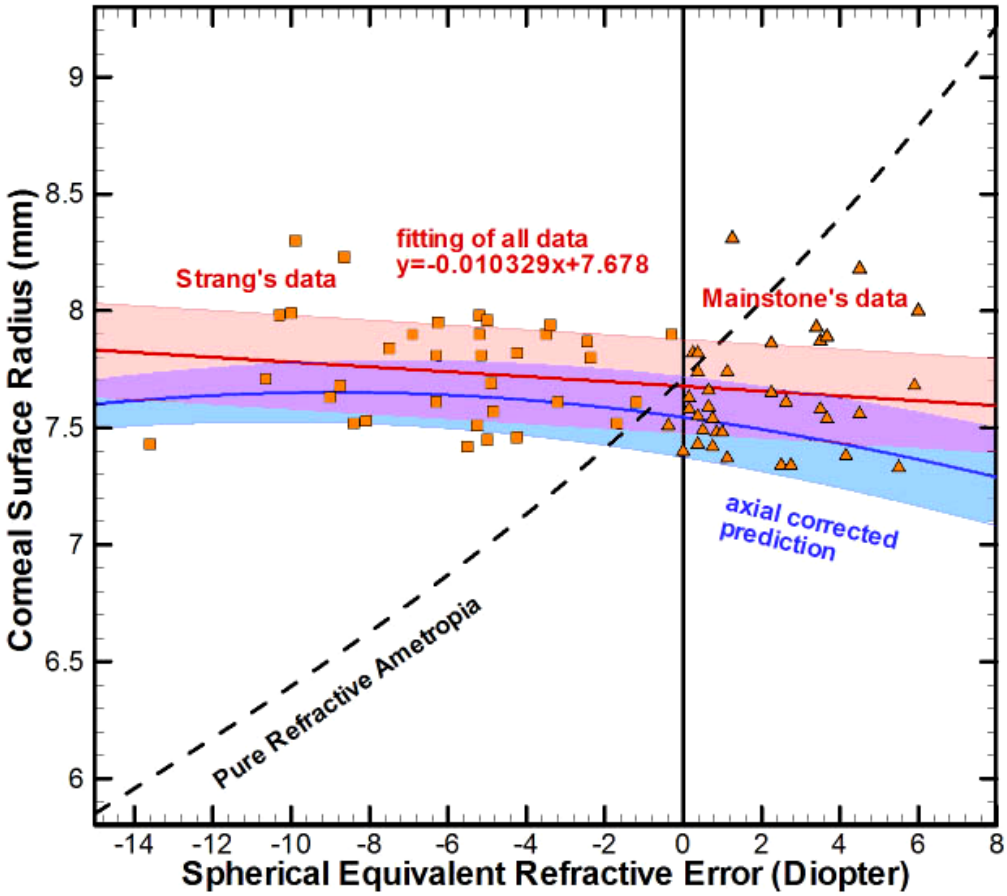

Figure 2.12 Radius of outer cornea surface vs. refractive error.

become the solid blue line in Figure 2.12. The light-blue band around the blue axial-corrected prediction line is the corresponding distribution (pink band) from axial relation obtained in Figure 2.11. The blue band region calculated from the axial corrected model is now much closely resembled to the measured data of the pink band area. This encouraging result leads to a general ametropic eye model that includes all three cause factors. One interesting result from the measured data in Figure 2.11 and 2.12 is concerned with the correlation between axial length and cornea curvature. The axial length contributes to the refractive error dominantly as indicated in the comparison between pure axial eye model and measured data in Figure 2.11. The relation of cornea curvature vs. refractive error, however, goes in the opposite direction (slopes) between the measured data (red line) and the pure refractive (curvature) model (black dashed line). This observation implies that the shortening (or lengthening) of the eyeball results to hyperopia (or myopia) while the radius of cornea surface decreases (or increases) in the sense to reduces the degree of hyperopia (or myopia). From the Viewpoint of eye geometry, when the axial length of eye increases, though not proportionally, the lengths of the other dimensions including the cornea radius increase, imposes an opposite influence in refractive error. Roughly, for every diopter incremental increase of refractive error, the axial length decreases 1.73% and the cornea radius decreases only 0.135 % in average. The distribution of ocular axial length is about 3.4% of average length and cornea radius distribution is about 5% of average value.

To establish a general ametropic human eye model that includes all three types of causal factors, the fitted relations of axial length and cornea curvature versus refractive error (the red solid lines and pink band in Figure 2.11 and Figure 2.12) are adopted into

the simulation. The intraocular power in the pupil location is used to compensate the remanding refractive error. The relationship between the required virtual lens power and refractive error is therefore obtained as the solid blue line shown in Figure 2.13. The light- blue band in Figure 2.13 is the corresponding distribution calculated from the 50% distribution bands in Figure 2.11 and 2.12. Assuming the distributions in axial length and cornea curvature are normal distributions, this blue band area should cover about 80 % of distribution. Since the intraocular measurement including gradient refractive index is difficult to acquire in vivo, it is reasonable to assume and use one single variable, the power of a virtual lens, to represent the intraocular power contribution. The calculation of the required intraocular power for all measured data point are performed and the results are illustrated as triangle and square symbols in Figure 2.13. The proposed general ametropic eye model (blue line and band) shows great agreement with the measured data from literature. The final general ametropic eye model can therefore be described in Figure 2.14 and 2.15. In Figure 2.14, for an eye with specific refractive error, the corresponding axial length, cornea radius, and intraocular power compensation are indicated in red, blue, and green lines, respectively. The shaded areas indicate the variation in population differences. One thing to be noticed is that the emmetropic eye (zero refractive error) of this general ametropic eye model has a ~1 diopter virtual lens and slightly different parameters of axial length and cornea radius deviated from the Navarro model. Figure 2.15 illuminates the dioptric contribution of the axial length, cornea radius and intraocular power to the refractive error. The shaded areas (bands) around the curves correspond to the distribution of indicated percentages. The axial length contributes the majority of refractive error while the cornea reduces the degree of

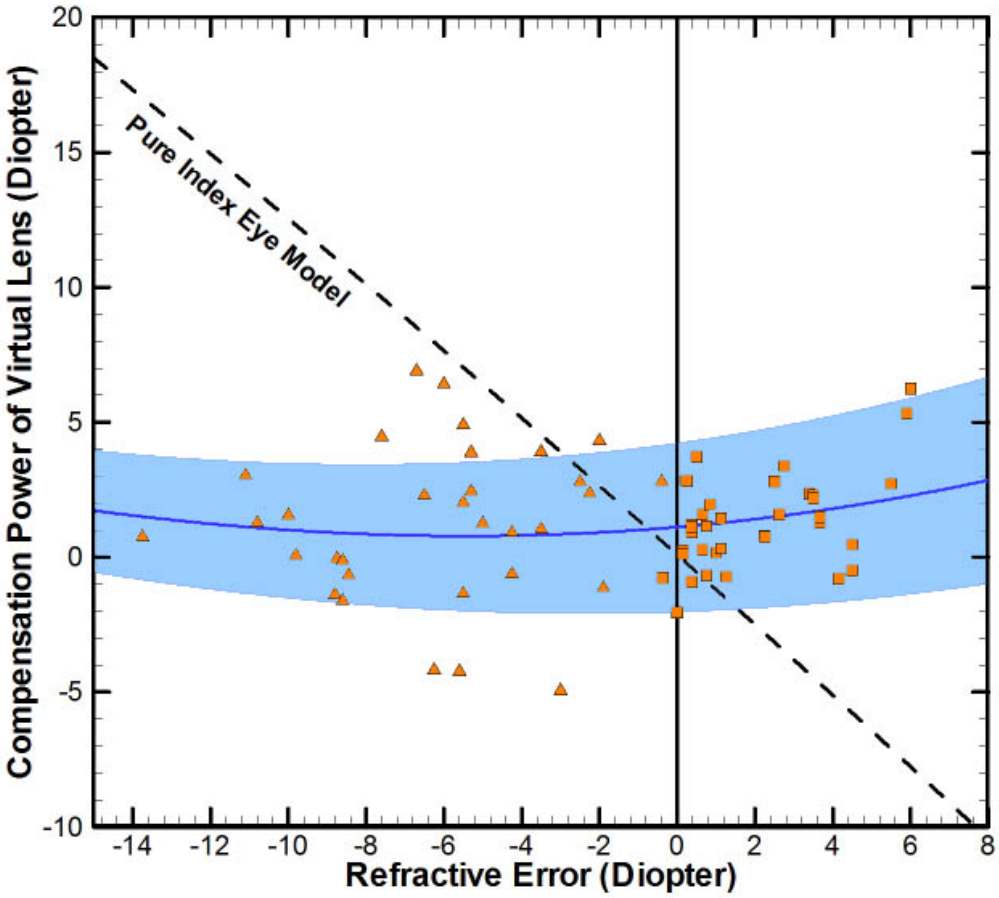

Figure 2.13 The relationship between corneal radius of curvature and refractive error

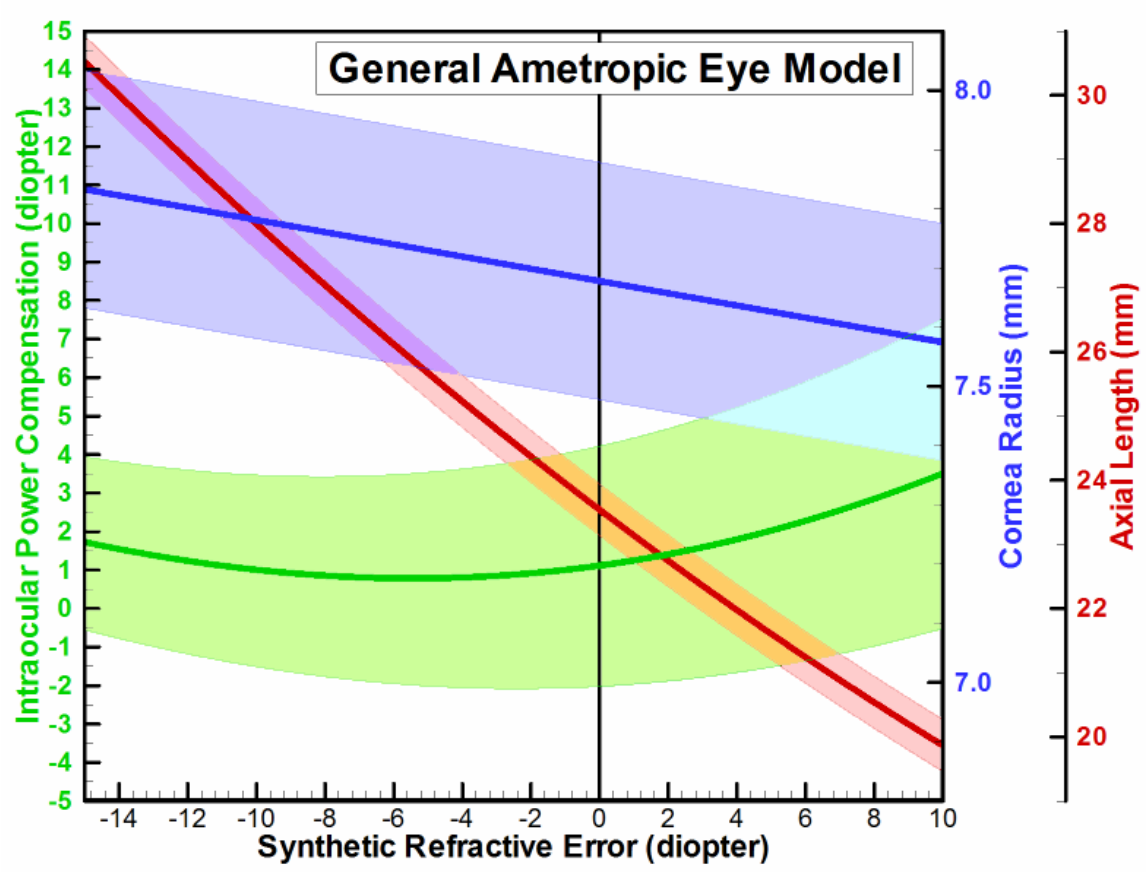

Figure 2.14 Variables used in the general ametropic eye model

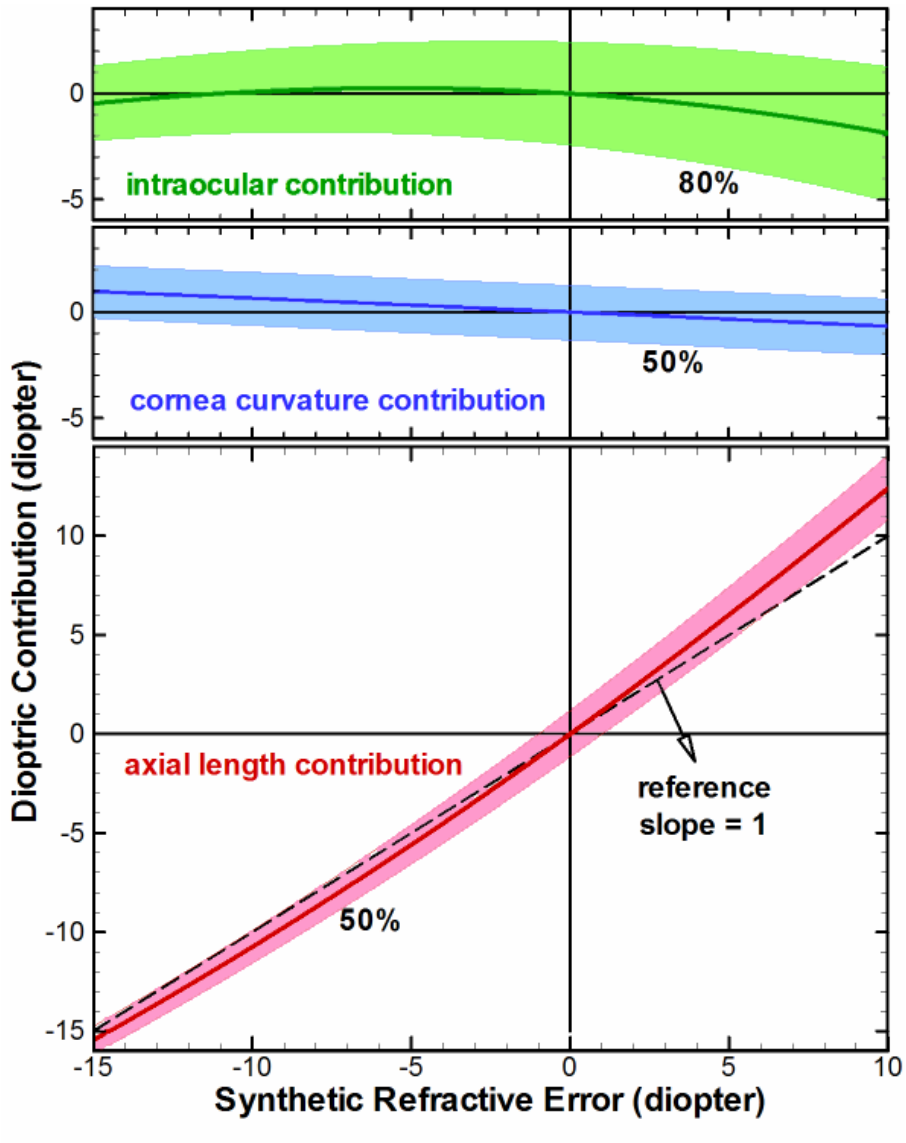

Figure 2.15 Dioptric contributions of three cause-factors in the general eye model

refractive error slightly. The distribution bands in both Figure 2.14 and 2.15 allow the simulation to be performed for variation in large group of subjects.

Chapter 3

The performance of ametropic model eye

In the previous chapter, a general ametropic eye model was constructed according to the published statistics of experimental data. In this chapter, the performance of this eye model was investigated and compared with published measured aberration data from human subjects.

Aberrations are the measures of imaging imperfections of an optical system. They define the departures from the idealized Gaussian optics, or paraxial prediction. One distinguished type of aberration is chromatic aberration (CA). CA arises from the fact that the refractive index of the optical media varies with wavelength. In human eyes, chromatic effect results to as large as 2 diopters difference in focusing power across the range of visible light. Monochromatic aberration, on the other hand, is the term of all types of aberrations that are independent of wavelength. In most optical design books, especially for evaluating an optical element or system, Seidel aberration coefficients are used to identify types of monochromatic aberrations and to assist improving optical design. For a rotationally symmetric optical system, which is mostly the case, even orders of Seidel aberrations vanish. In general, the lower-order aberrations are more announced

in an optical system than higher order ones. The first order of Seidel coefficient represents the defocus, the displacement of focusing plane. It is exactly the refractive error or the ametropic condition in ocular system. The third-order and higher-order Seidel aberrations are sorted into five famous groups: spherical aberration (S_1), coma (S_2), astigmatism (S_3), Petzval field curvature (S_4), and distortion (S_5). Spherical aberration (S_1) is the only on-axis aberration among the five. This imperfection results from the increase of pupil size of the system that breaks the paraxial approximation. Since the object is on the visual axis and the image is expected to fall right onto fovea, spherical aberration affects optical performance just next to defocus. Coma (S_2) and astigmatism (S_3) are aberrations of defected focusing due to combined effects of pupil size and the field angle. If an optical system is designed to be free of these three types of aberrations, S_1 - S_3, a point to point focusing becomes possible. Petzval field curvature (S_4) and distortion (S_5) do not refer to focusing defects. They represent misplaced imaging that is either on a curved surface, deviated from the expected imaging plane (S_4), or is spatially distorted image on the expected plane (S_5).

Other than Seidel interpretations, wavefront aberration (*WFA*) is an alternative way of evaluating performance of an optical system. *WFA* is defined as the optical path difference (OPD) between the real wavefront and a reference or perfect wavefront (normally the spherical wavefront projected from a desired imaging point) as a function of position on the exit pupil. This two dimensional function of *WFA* is normally expended into Zernike polynomial function series. Zernike interpretation has several useful features in optometry and recently has gained considerable popularity in community of vision science. In the following sections, the chromatic aberration, on-axis

and off-axis Seidel aberrations and wavefront aberrations of the general ametropic eye model were discussed.

3-1. Chromatic aberration

Study of chromatic aberration in the schematic eye provides a valuable guide to the performance of the living eye. It is essential for simulation of ocular measurement using instruments with light source in specific wavelength range such as infrared or broad spectrum. Longitudinal chromatic aberration (*LCA*) is the measure of the refraction deviation of the system between light with wavelength, λ, and a reference wavelength, λ_o. Figure 3.1 shows the theory of one method to measure the chromatic difference of refraction, longitudinal chromatic abberation (*LCA*), in the small region of pupil (dia=3mm). If two small or narrow test objects placed at *T1* and *T2* and illuminated by red and blue light, respectively, both would be imaged at fovea. To the observer, they would thus appear to be coincident. Therefore, if we choose a wavelength (wavelength of red light in Figure 3.1, but usually green light of 555nm is chosen) λo as a reference wavelength, *LCA* is normally expressed in *diopter*, or *meter* $^{-1}$, as

$$LCA(\lambda) = \frac{n(\lambda)}{l(\lambda)} - \frac{n(\lambda_o)}{l(\lambda_o)} \ , \tag{3.1}$$

where n is the refractive index of air ($\approx$1) and l is the object distance, indicated at the Figure 3.1. The *LCA* calculation from equation (3.1) was performed for 21 ametropic conditions from +10 to -10 diopters of the general eye model. The result was shown with measured data reproduced from published papers [Thibos (1992), Charman (1976), Lewis (1982) and Wald (1947)] in Figure 3.2. The *LCA* of general eye model agreed with the

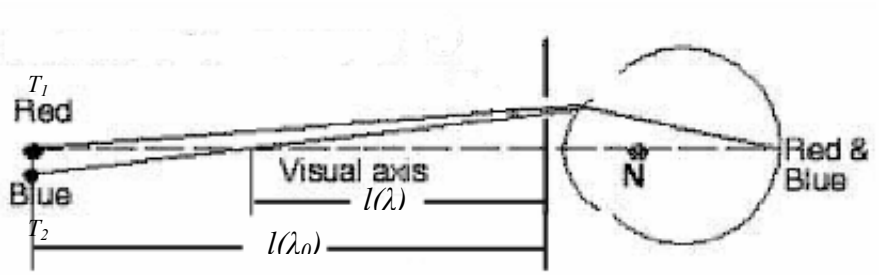

Figure 3.1 Measurement of *LCA* in object space

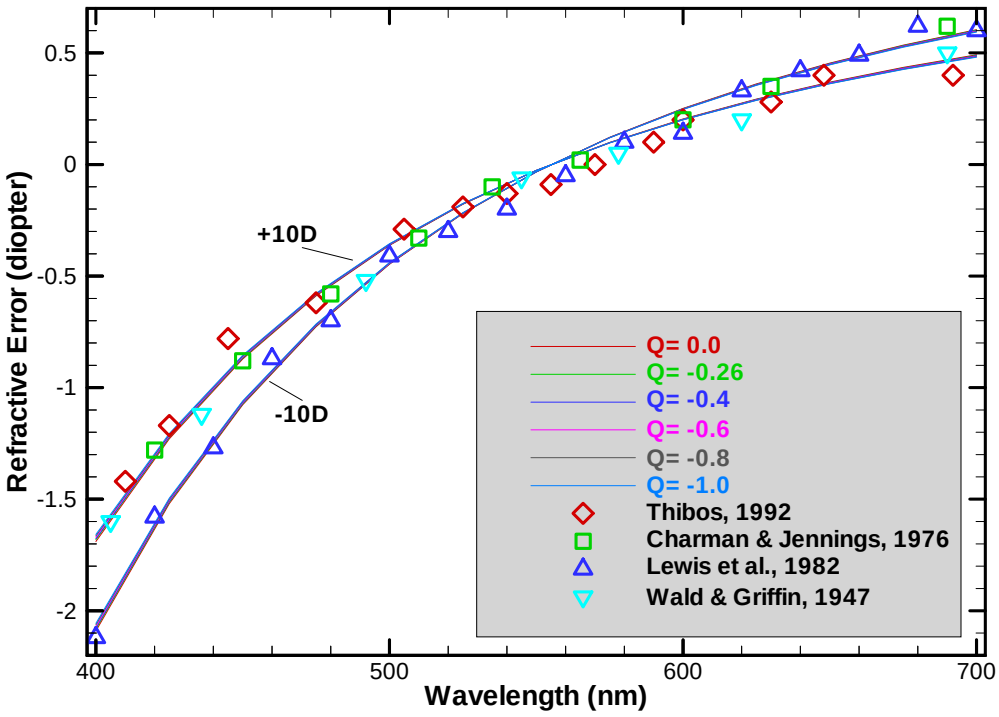

Figure 3.2 Comparison of longitudinal chromatic aberration of general eye model and published data. [Thibos (1992), Charman (1976), Lewis (1982) and Wald (1947)]

measured data within the error range of measurement. The chromatic aberration appeared to be affected by refractive status. The *LCA* of our general model appears to be greater in myopes than hyperopes for fixed conic constant. However, when the power of the eye is fixed, the conic constant *Q* only changes *LCA* a tiny bit. Considering the small range of variation, chromatic effects of human eye can be predicted using eye modeling with great confidence if the refractive status for reference wavelength is known.

3-2. Seidel aberrations

For on-axis optical performance, other than defocus, spherical aberration is believed the most significant aberrations. In previous chapter, the general ametropic eye model was constructed to provide any desired defocus conditions between +10 and -15 diopters. The quantity of refractive error was calibrated under paraxial condition or small pupil diameter near 2- to 3-mm. The conic constant, which described the asphericity or the periphery flattening of cornea surface, has little effect to the ametropic condition. When the pupil size increased, the performance of eyes was expected to be affected by not only the cornea curvature but also the asphericity. This degradation of imaging quality could be evaluated and quantified with Seidel spherical aberration (SA) that would be discussed in this section.

For off-axis imaging, combined with spherical aberration and defocus, oblique astigmatism and coma were most significant. To examine the effect of field angle upon ocular imaging, astigmatism was calculated and presented for the general ametropic model eye following the discussion of SA over a range of field angle.

Longitudinal Spherical Aberration

Longitudinal spherical aberration (*LSA*) is defined as the difference of the dioptric distances (in *meter* $^{-1}$ = *diopter*) between the paraxial and marginal foci, f_p and f_r, measured from the second principal plane of the optical system (see Figure 3.3). In ocular system, the expression of *LSA* as a function of *r*, the distance from optical axis, is illuminated in the equation (3.2)

$$LSA(r) = \frac{n'}{f_r} - \frac{n'}{f_p} \ , \qquad (3.2)$$

where *n'* is the refractive index of aqueous humor. A positive value of the *LSA* denotes uncorrected spherical aberration or relative myopia. An over-corrected spherical aberration indicated a negative *LSA*. Using equation (3.2), *LSA* of the general ametropic eye model was calculated and shown in Figure 3.4 for various values of conic constant *Q* from -1.0 (parabola, in light blue lines) to 0 (spherical surface, indicated with red lines). As the result indicated, for a fixed conic constant, the degree of refractive error affects *LSA* little although the axial length and cornea curvature varied with refractive error. However, the conic constant, *Q*, of the cornea front surface affected *LSA* dramatically. For *Q* = 0, the spherical corneal, *LSA* reached higher than 4 diopters for rays entered at 4 mm from center of cornea. For *Q* = -1.0, the parabolic surface, and *Q* = -0.8, elliptical surface, *LSA* was over-corrected. The shaded area around each colored group of calculation marks the distribution spread caused by the variation of axial length and cornea radius

Comparison of *LSA* of some published eye models with the general ametropic model was given in Figure 3.5. In the figure, gray-shaded areas on the background

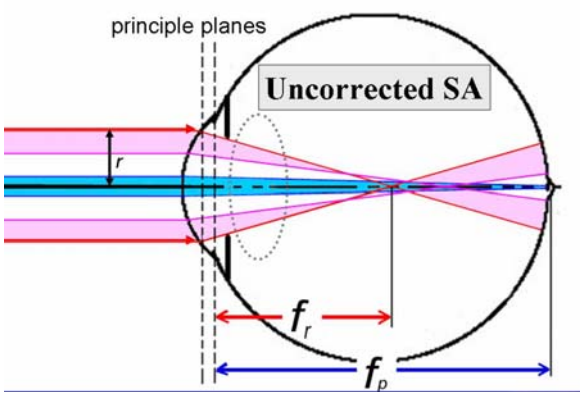

Figure 3.3 Spherical aberration, a measure of the on-axis power deviation of an optical system caused by pupil size.

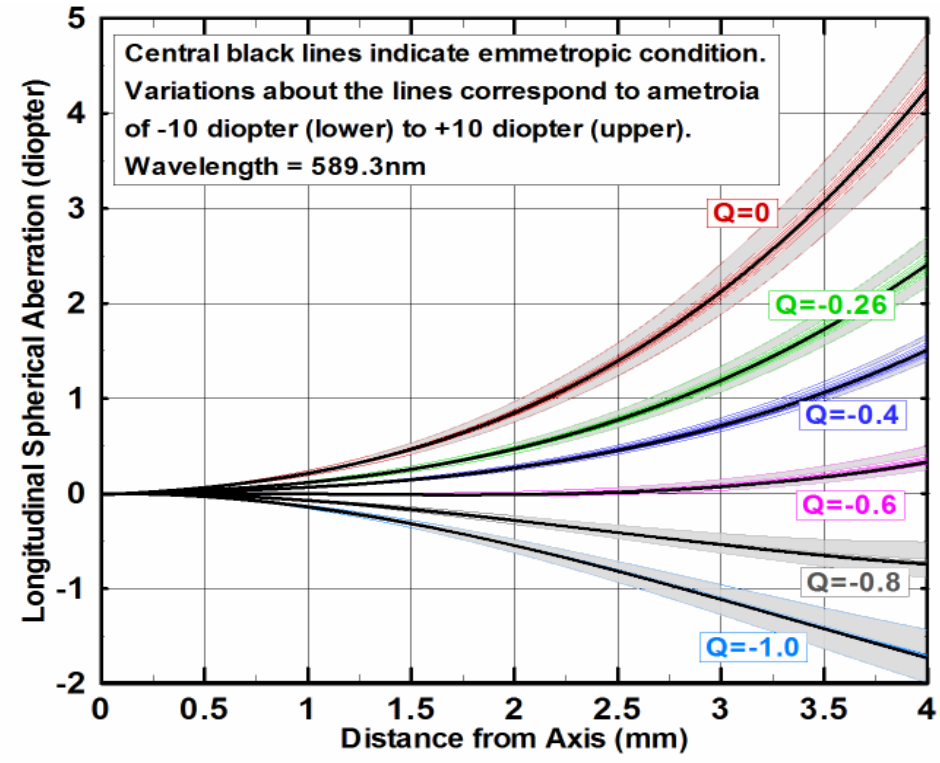

Figure 3.4 Longitudinal spherical aberration of the general ametropic eye model.

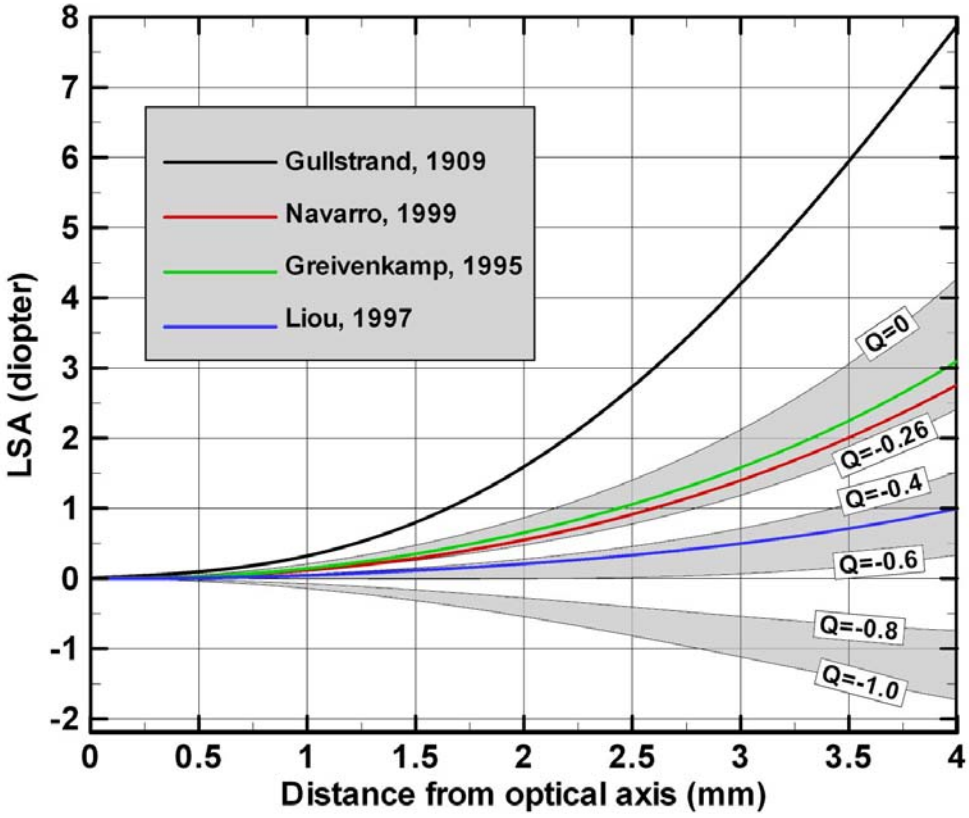

Figure 3.5 Comparison of *LSA* of published eye models.

marked *LSA* curves of general eye model as solid black lines in Figure 3.4. The *LSA* curve of Navarro eye model was plotted as a red line, which was separated from the $Q = -0.26$ line of the new model. The Liou model (blue line) exhibited a much smaller *LSA* compared to others. These two models were constructed according to measured *LSA* data, which were obviously different from each other. If Navarro-, Greivenkamp-, and Liou-models represent the range of typical spherical aberration condition of adult eyes, a conic constant around -0.1 to -0.5 should be adopted in the general eye model.

Measurement of spherical aberration was not easy to perform especially in the alignment of visual axis with sufficient accuracy. Some of the *LSA* measurement results were reproduced in Figure 3.6. Among them, van Meeteren's data are the result of a curve fitting to the experimental data available in the literature at that time; Thibos adjusted the shape of a single-surface reduced eye to reproduce experimental values of *LSA*. Unfortunately, unlike chromatic aberration, ocular spherical aberration varies considerably from person to person. As indicated from results of Ames [Ames (1921)] and Jenkins [Jenkins (1963)] in Figure 3.6, spherical aberrations measured from the four ocular quadrants of an individual were hardly the same. This was primarily due to the axial asymmetry nature of cornea surface. The studies of Jenkins in 1963 [Jenkins (1963)] and Cornsweet in 1970 [Cornsweet (1970)] also showed that spherical aberration was mostly over-corrected (negative) for very young children and it tended to increase with age. When children reached 6-8 year of age, *LSA* gradually converted to uncorrected type (positive). Although most adult eyes were with uncorrected spherical aberration, when accommodated, the amount of spherical aberration reduced and sometimes changed to the over-corrected type [Koomen (1949)]. Thibos adjusted the shape of a single-

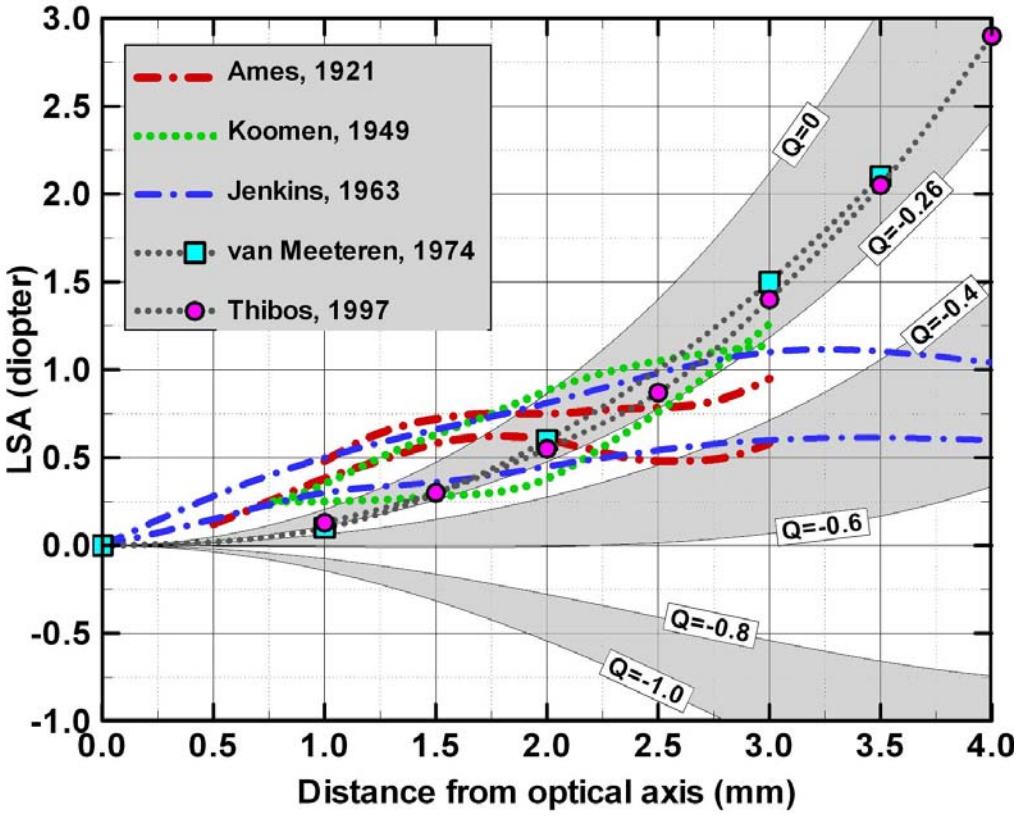

Figure 3.6 Measured *LSA* results from published literature. The upper curve line of Ames' data was the measurement for lower quadrant and the lower curve line was for the temporal quadrant of the same patient. The 2 lines of Koomen's result were measured from 2 patients. The upper and lower curve lines of Jenkins result were measurement for lower and upper quadrants of the same patient. The gray bands in the background were calculated from the general eye model. [Ames (1921), Koomen (1949), Jenkins (1963), Van Meeteren (1974) and Thibos (1997)]

surface reduced eye to reproduce experimental values of *LSA*; in contrast our schematic eye reproduces the same *LSA* using anatomical data without any fitting. For these reasons, it is wise to keep the conic constant a variable in the general eye model so that the simulation can be performed for variation of *LSA* according to the pupil size, age, and accommodation status.

Seidel Astigmatism

For off-axis imaging, combined with spherical aberration and defocus, oblique astigmatism and coma were most significant. To examine the effect of field angle upon ocular imaging, astigmatism was calculated and presented for the general ametropic model eye over a range of field angle.

The region of human vision defined by fovea, the best-resolution area on retina, represents a visual field of view (FOV) of about 1 degree. Within this region the normal eye will achieve a visual acuity or resolution of 1 arc minute. This on-axis optical performance was determined by the defocus and spherical aberration discussed previously. Outside this 1-degree field, the acuity of eye falls rapidly. The field of view of a typical human eye is about 170 degrees in horizontal and 140 degrees in vertical directions. The overlapping area that specifies binocular vision spans a field of view of about 140 degrees in both horizontal and vertical directions centered on the 2 visual axes. To evaluate the off-axis optical performance (side-view or peripheral vision) of the general ametropic model eye, Seidel longitudinal astigmatism (*LAST*) was investigated. *LAST* measured the power difference between tangential and sagittal foci as shown in Figure 3.7. The mathematics expression of *LAST* was given in equation (3.3).

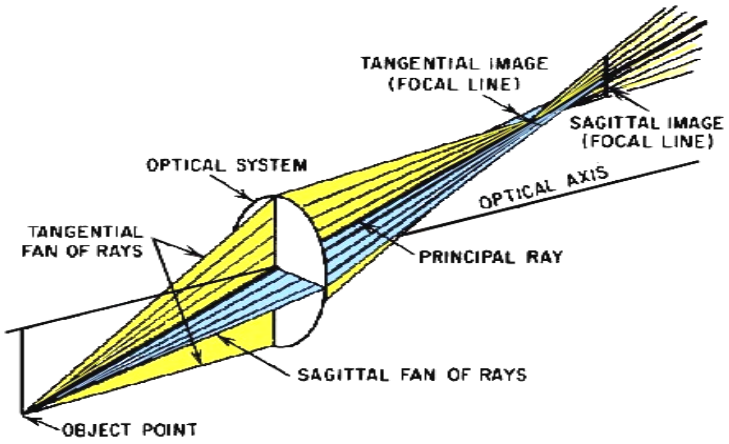

Figure 3.7 Seidel astigmatism

$$LAST(\theta) = \frac{n'}{f_t} - \frac{n'}{f_s}, \tag{3.3}$$

where n' was refractive index of aqueous humor, f was the focus distance from the second principal plane, and the subscripts t and s indicated tangential and sagittal respectively. The calculation result of *LAST* is shown in colored solid lines in Figure 3.8. The different colors from red to violet represent the periphery flattening degree of cornea described by conic constant Q. For each conic constant, refractive errors of -10 diopters to +10 diopters are calculated. As shown in the figure, the refractive status does not affect side-vision much. The conic constant has much more influence to this aberration, as it does to spherical aberration. If the relation between conic constant and spherical aberration described in last section is direct, children under 7 year-old would have typical conic constant of < -0.7 (blue and violet lines in Figure 3.7), a condition that refers to much better side-vision than adults according to the calculation result. In the same figure, *LAST* of 2 published eye models from Navarro in 1985 [Navarro 1985] and

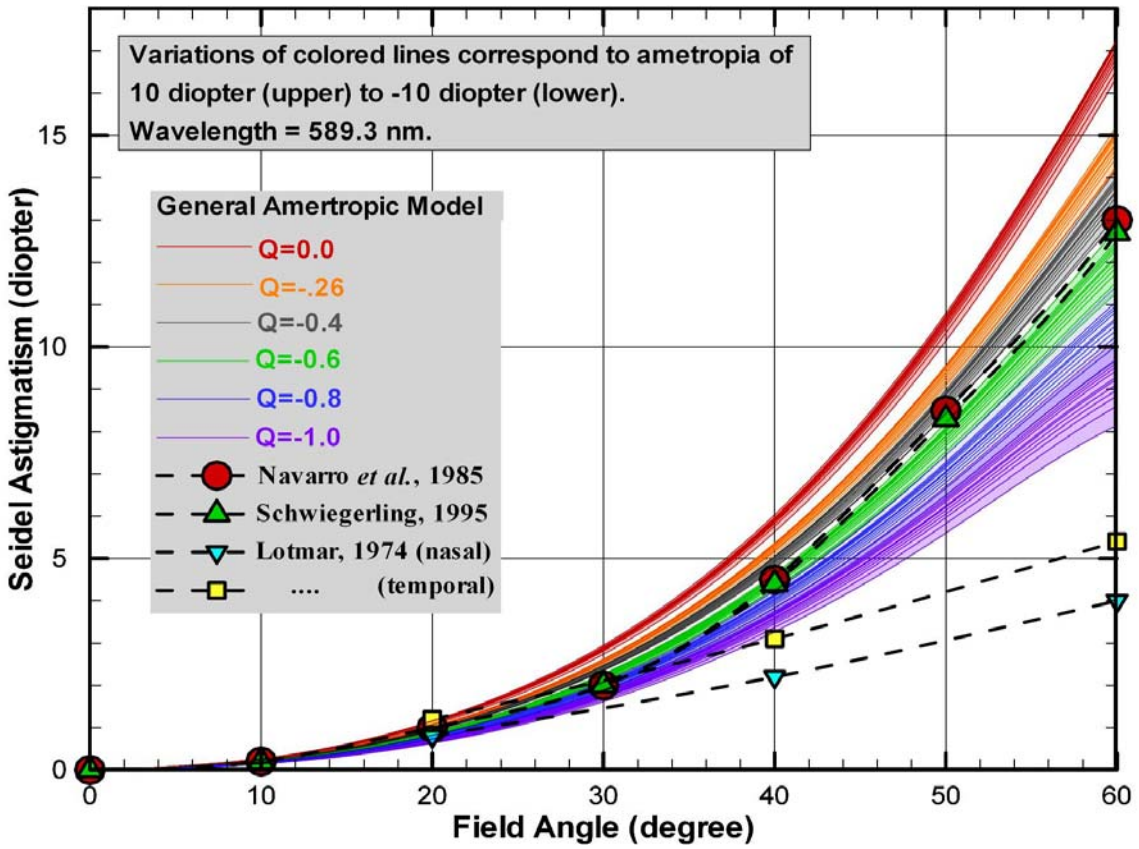

Figure 3.8 Seidel Astigmatism of general ametropic eye model and the comparison with published literature

Schwiegerling in 1995 [Schwiegerling 1995] are also plotted in red circular and green delta symbols. Their eye models fall in the region of $Q \approx -0.5$. The only measured *LAST* data that we found is from Lotmar in 1974 [Lotmar 1974]. The nasal and temporal data shown in the figure are the average of measured data. The mismatch of *LAST* at field angle greater than 30 degree will be discussed later in the wavefront aberration section.

3-3. Wavefront aberration

Other than Seidel interpretations, wavefront aberration (*WFA*) is an alternative way of evaluating monochromatic performance of an optical system. *WFA* is defined as the optical path difference (OPD) between the real wavefront and a reference or perfect wavefront as a function of position on the exit pupil. A wavefront indicates the surface of a constant optical path. The wavefronts of a point source in space are a sequence of spherical surfaces moving outward. For a perfect un-accommodated eye, the retinal surface conjugates to the plane at infinity. Assuming a point source located on retinal surface of a perfect eye, the wavefront emerges as a plane-wave at the exit pupil. As shown in Figure 3.9, *WFA* of an eye can be measured experimentally by projecting a laser beam onto retina to form a diffusive point source. The rays from the point source travel through the elements of eye and exit the cornea. The 2-dimensional wavefront at the exit pupil is collected and compared with the ideal wavefront, the plane wave in this case, to obtain the point to point difference, $W(\rho, \theta)$, where $\rho = r/r_{max}$ is the normalized distance from the centre of exit pupil and θ is the azimuth angle (ρ and θ are illuminated in the Figure 3.9) . Wavefront aberration is usually expressed in μm or wavelength, λ, and

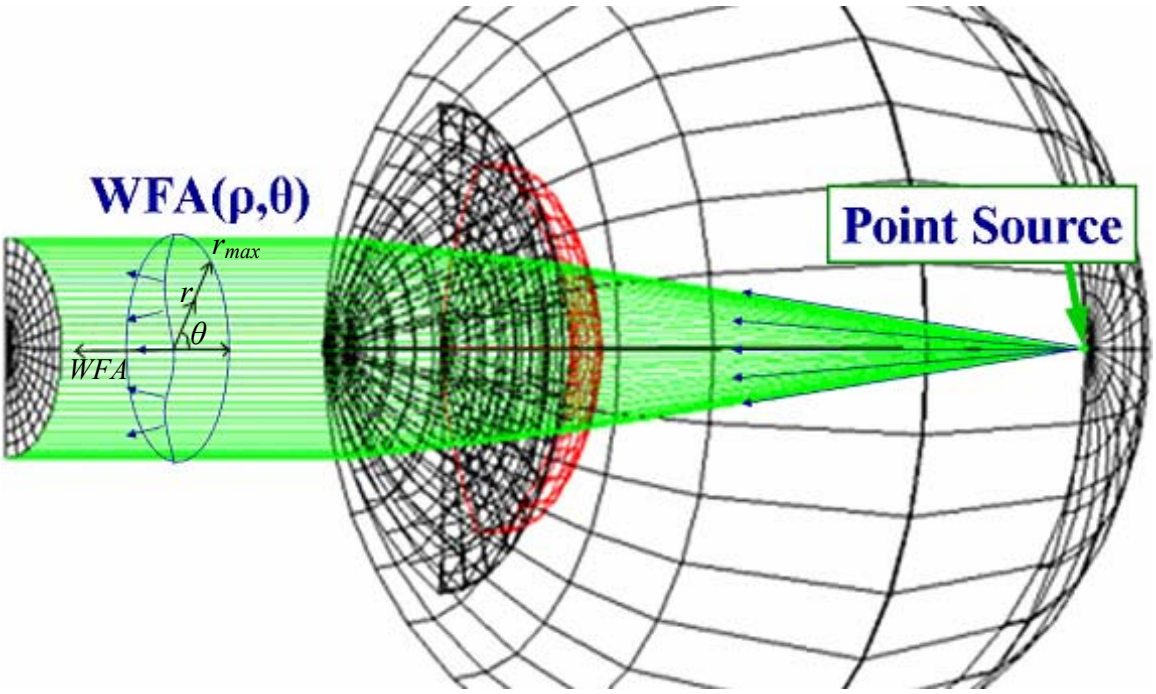

Figure 3.9 Diagram of wavefront aberration in ocular system.

often is assigned to be zero at the center point, i.e. $W(\rho=0)=0$. It is comprehensible to describe *WFA* in wavelength since the destructive interference occurs when $W(\rho, \theta)> \lambda/2$.

Zernike polynomial functions are normally used to describe the 2-dimensional *WFA* function. Zernike polynomial functions, $\{Z_n^m\}$, represent a completely orthonormal set of functions that can be used to describe any 2 dimensional functions in a normalized polar coordinate. The mathematic form of Zernike function is

$$Z_n^m(\rho,\theta) = \left\{ \begin{array}{l} N_n^m R_n^{|m|}(\rho)\cos(m\theta), \text{ for } m \geq 0 \\ N_n^m R_n^{|m|}(\rho)\sin(|m|\theta), \text{ for } m < 0 \end{array} \right\}, \quad (3.4)$$

where

$$R_n^{|m|}(\rho) = \sum_{s=0}^{(n-|m|)/2} \frac{(-1)^s (n-s)!}{s![0.5(n+|m|-s)]![0.5(n-|m|-s)]!} \rho^{n-2s}, \quad (3.5)$$

and N_n^m is the corresponding normalization constant. The indexes, n and m, in Zernike function indicate the highest power of normalized radius and the frequency of azimuthal angle respectively. 2-dimensional maps of Zernike functions are plotted in Figure 3.10. Table 3.1 gives the first 28 Zernike functions. The aberration names and number 0 to 20+ in the Table 3.1 and Figure 3.10 were announced as standard by Optical Society of America (OSA) in 1999 to present human eye aberrations [Thibos (2002)]. The same system was also adopted by the American National Standards Institute in 2004 [American National Standards, 2004]. It is very important to point out that although the names of Zernike polynomial aberrations in Table 3.1 appear to be the same as names in Seidel aberrations, they do not imply the same things. For example, coma and astigmatism in Seidel aberrations system are measures of errors caused by the existing of field angle.

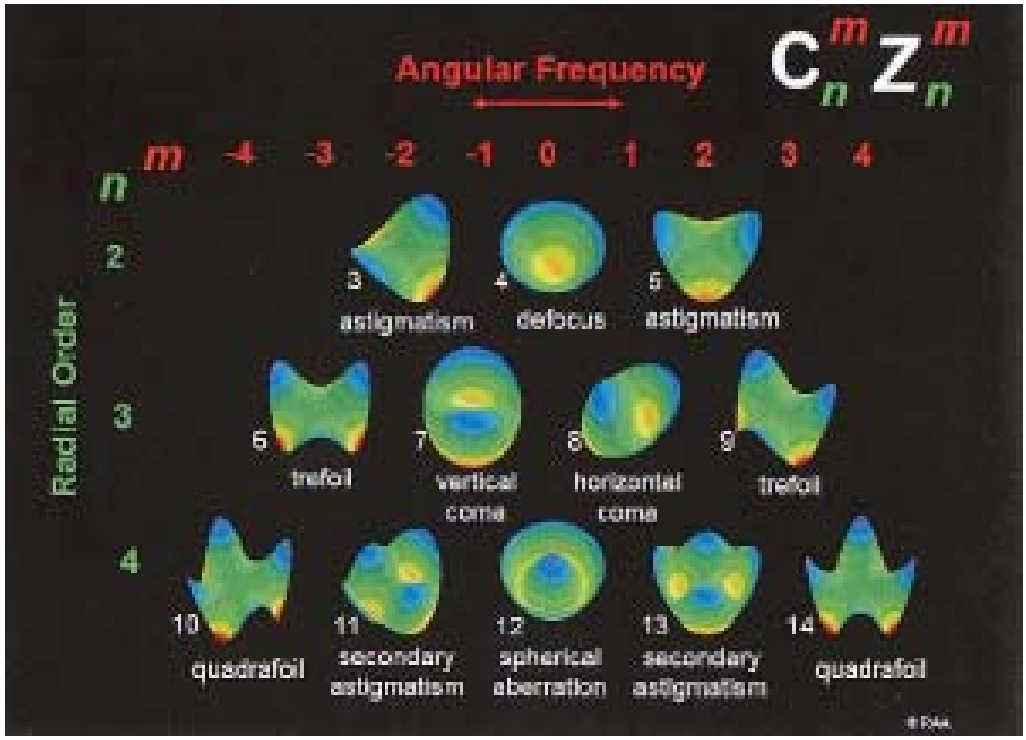

Figure 3.10 Zernike expansion showing the 2nd, 3rd, and 4th radial order modes using the Optical Society of America (OSA) recommended notation. [Applegate, 2003]

Table 3.1. Zernike polynomial function

#	Zernike func	Characteristic	Polar presentation
0	Z_0^0	Piston	1
1	Z_1^{-1}	Vertical tilt	$2\rho \sin(\theta)$
2	Z_1^1	Horizontal tilt	$2\rho \cos(\theta)$
3	Z_2^{-2}	Oblique astigmatism	$\sqrt{6}\,\rho^2 \sin(2\theta)$
4	Z_2^0	Defocus	$\sqrt{3}\,(2\rho^2-1)$
5	Z_2^2	With-/against-the-rule astigmatism	$\sqrt{6}\,\rho^2 \cos(2\theta)$
6	Z_3^{-3}	Oblique trefoil	$\sqrt{8}\,\rho^3 \sin(3\theta)$
7	Z_3^{-1}	Vertical coma	$\sqrt{8}\,(3\rho^3-2\rho) \sin(\theta)$
8	Z_3^1	Horizontal coma	$\sqrt{8}\,(3\rho^3-2\rho) \cos(\theta)$
9	Z_3^3	Horizontal trefoil	$\sqrt{8}\,\rho^3 \cos(3\theta)$
10	Z_4^{-4}	Oblique quatrefoil	$\sqrt{10}\,\rho^4 \sin(4\theta)$
11	Z_4^{-2}	Oblique secondary	$\sqrt{10}\,(4\rho^4-3\rho^2) \sin(2\theta)$
12	Z_4^0	Spherical aberration	$\sqrt{5}\,(6\rho^4-6\rho^2+1)$
13	Z_4^2	With/against rule secondary astigmatism	$\sqrt{10}\,(4\rho^4-3\rho^2) \cos(2\theta)$
14	Z_4^4	Quatrefoil	$\sqrt{10}\,\rho^4 \cos(4\theta)$
15	Z_5^{-5}		$\sqrt{12}\,\rho^5 \sin(5\theta)$
16	Z_5^{-3}		$\sqrt{12}\,(5\rho^5-4\rho^3) \sin(3\theta)$
17	Z_5^{-1}	Secondary vertical coma	$\sqrt{12}\,(10\rho^5-12\rho^3+3\rho) \sin(\theta)$
18	Z_5^1	Secondary horizontal coma	$\sqrt{12}\,(10\rho^5-12\rho^3+3\rho) \cos(\theta)$
19	Z_5^3		$\sqrt{12}\,(5\rho^5-4\rho^3) \cos(3\theta)$
20	Z_5^5		$\sqrt{12}\,\rho^5 \cos(5\theta)$
21	Z_6^{-6}		$\sqrt{14}\,\rho^6 \sin(6\theta)$
22	Z_6^{-4}		$\sqrt{14}\,(6\rho^6-5\rho^4) \sin(4\theta)$
23	Z_6^{-2}		$\sqrt{14}\,(15\rho^6-20\rho^4+6\rho^2) \sin(2\theta)$
24	Z_6^0	Secondary spherical	$\sqrt{7}\,(20\rho6-30\rho4+12\rho^2-1)$
25	Z_6^2		$\sqrt{14}\,(15\rho^6-20\rho^4+6\rho^2) \cos(2\theta)$
26	Z_6^4		$\sqrt{14}\,(6\rho^6-5\rho^4) \cos(4\theta)$
27	Z_6^6		$\sqrt{14}\,\rho^6 \cos(6\theta)$

Without a limited field of view, these two aberrations are zero. The wavefront aberration is measured without field angle or corresponding field of view. For rotationally symmetric eye models, the azimuthal-angle dependent terms vanish; i.e. $C_n^{m\neq 0} = 0$. Spherical aberration, which depends significantly on pupil diameter, appears in C_4^0, C_6^0, C_8^0 terms and so on. The coma and astigmatism terms in Zernike coefficients ($C_n^{m\neq 0}$) illustrate the asymmetry property of the ocular system that has nothing to do with field angle. This ocular asymmetry potentially could affect the on-axis focusing quality. They become zero for a perfect rotationally symmetric system. In the Seidel system, coma and astigmatism describe the focusing quality of side view. They exist even when the optical system is rotationally symmetric.

The wavefront aberration, $W(\rho,\theta)$ of eyes can be expressed as the superposition of Zernike functions, $\{Z_n^m\}$, times their weighting coefficients, $\{C_n^m\}$.

$$W(\rho,\theta) = \sum_{n=0}^{k} \sum_{\substack{m=-n \\ n-|m|=even}}^{n} C_n^m Z_n^m(\rho,\theta). \qquad (3.6)$$

Therefore, the coefficients, $\{C_n^m\}$, can be used to represent *WFA* of an eye. Typically, the zero and first order coefficients present the degree of coordinate shift and tilt and the three coefficients in second order Zernike (C_2^{-2}, C_2^0, C_2^{+2}) correspond to the degree of ocular defocus. The Zernike coefficients with m=0, +2, -2 can be related mathematically to the clinical prescription of (*Spherical, Cylindrical, Axis*) in general. A calculation with the application of some of Zernike 2nd, 4th, 6th and 8th order coefficients to achieve ametropic condition was performed for ametropic eye models [Schwiegerling (1995a), Rainer (1998), Guirao (2003) and Atchison (2004)]. Figure 3.11 shows the result of our general ametropic eye model using Zernike coefficients. These results showed good

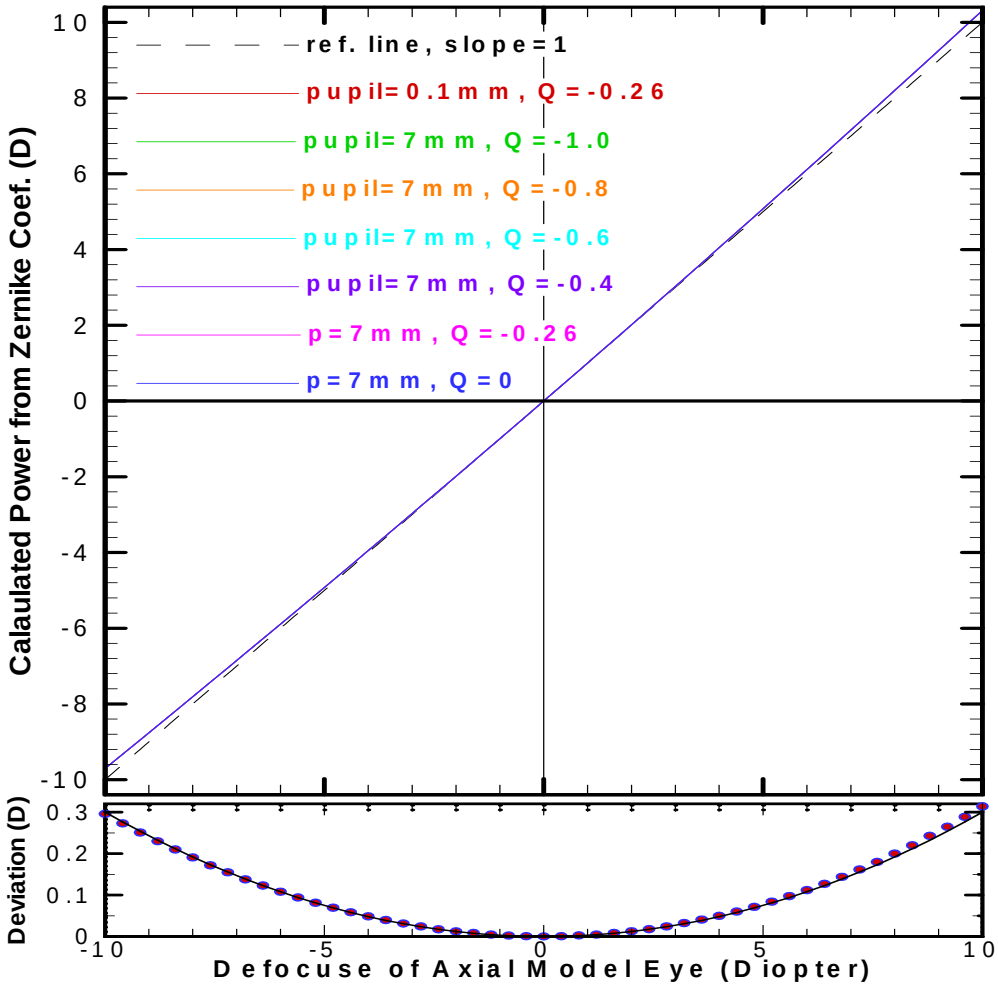

Figure 3.11 Defocus power of ametropic eye model obtained from Zernike 2nd and 4th order coefficients.

agreement with the refractive errors obtained from the ray tracing (far-point attempt). The deviation of Zernike method is about 1.5% at +5 and -5 diopters and about 3% at +10 and -10 diopters. The neglect of ρ^2-terms in higher order contributions would be the major cause of this deviation (see Table 3.1). One interesting thing is that the pupil diameter does not affect the Zernike-derived defocus result although the coefficients, $\{C_n^m\}$, strongly depend on the pupil size. As shown in Figure 3.11). the calculation was performed for pupil diameter of 7 mm and 0.1 mm for various Q values. All calculations led to the same defocus result. The Q number and the pupil size, however, do influence the far-point position. The Zernike derivation that omits high-order coefficients leads to a 'high-order-aberration free' condition, which is 'paraxial' or pupil-size independent.

Higher-order Zernike coefficients describe more complex asymmetry and radius dependence of eyes which can not be corrected with regular eye glasses or contact lens. As a matter of fact, the common corrections of defocus including eye glasses and contact lens and especially laser surgery (LASIK) could introduce additional higher order aberrations. Although high-order Zernike coefficients for eyes of majority population including ametropic eyes contribute very little to vision deficiency, these values increase for abnormalities such as keratoconus eyes or post laser surgeries (radial keratotomy, photorefractive keratectomy and automated lamellar keratoplasty, etc.), which exhibit irregular shaped cornea. By subtracting lower order contribution from the total wavefront aberration, the irregular feature of high-order aberrations shows. In this section, the wavefront aberration of general ametropic model is calculated and compared with measured data. It is of our interest to find out any correlations between refractive errors and high-order aberrations.

Measured RMS wavefront aberration (WFA)

In stead of the 2-dimensional function, $W(\rho, \theta)$, root mean square wavefront aberration (*RMS_W*) is a more straightforward representation of the imperfection degree of the ocular system. A direct derivation of the RMS of *WFA* leads to the simple relation of Eq. (3.7) by adopting the orthornormal property of Zernike polynomials.

$$RMS\_W = \sqrt{\sum_n \sum_m (C_n^m)^2} = \sqrt{\sum_n C_n^2} \quad . \tag{3.7}$$

As the equation indicates, the aberration contribution from each individual Zernike order is accumulated in a simple and comprehensible manner.

During the past many years, measurement on *WFA* of human eyes became achievable for many facilities and their correlations with age, accommodation status, or geometrical parameters of the eye were investigated by many research groups [Llorente (2004), Amano (2004), Wang (2003), Kuroda (2002), Cheng (2003), McLellan (2001), He (2000), Atchison (1995) and Collins (1995)]. Unfortunately, research result that links refractive error to wavefront aberration is far from sufficient. In a recent study of this ametropia-correlation performed by the School of Optometry in Indiana University [Cheng (2003)] *WFA* of 200 eyes of 100 young subjects were measured. The average age of subjects was 26.1 ± 5.6 year-old. Accommodation was paralyzed and pupils were dilated. No eye had pathology. The spherical component of refractive error determined from subjective refraction ranged from +5.25D to –9.50D and astigmatism ranged from 0 to –3.50D. The two eyes of the same subject were treated separately. Zernike analysis was performed based on a 6-mm diameter entrance pupil. From the fitted Zernike coefficients (averaged from three trials) total RMS wavefront error, as well as the RMS

aberrations in 3rd (coma) and 4th (spherical aberration) orders were calculated. The distributions of these various measures across refractive error groups were evaluated statistically with linear regression and one way ANOVA ($p < .05$ significance level). The relationships between *RMS_W* and equivalent spherical refractive error are reproduced and shown in Figure 3.12 for their study population. Figure 3.12 shows refractive error-correlation of RMS_*W* of (A) high-order aberrations (HOA) including 3rd-order to 10th order, (B) 3rd-order, (C) 4th-order, and (D) spherical aberration (C_4^0 term). The regression slopes are given in each plot. The indexes, *m*, *p*, and *r* in the plots are regression slope, correlation coefficient, and significance of correlation respectively. Wavelength of light source is 632.8 nm in the study. The result of this study shows no significant correlation found for either the 3rd, the 4th, spherical aberration, or HOA with ametropic condition of human eye. There was also no evident ametropic-correlation or difference in distribution were observed between high astigmatism (> -1 diopter, open symbols in Figure 3.12) and low astigmatism (≤ -1 diopter, closed symbols in Figure 3.12) groups. Further, even when the subjects were classified into six different groups according to their refractive errors, the regression slopes of *RMS_W* in the examined orders were not much different. In conclusion, there was no observable correlation found between ametropic condition and *RMS_W* from the experimental investigation.

Calculated RMS WFA

To compare the performance of the synthetic ametropic model eye with the experiment data of *WFA*, the *RMS_W* was calculated based on 6-mm *WFA* analysis through the ametropic conditions and was shown in Figures 3.13 and 3.14. The calculation was performed for cornea conic constants from 0 to -1.0 as in section of

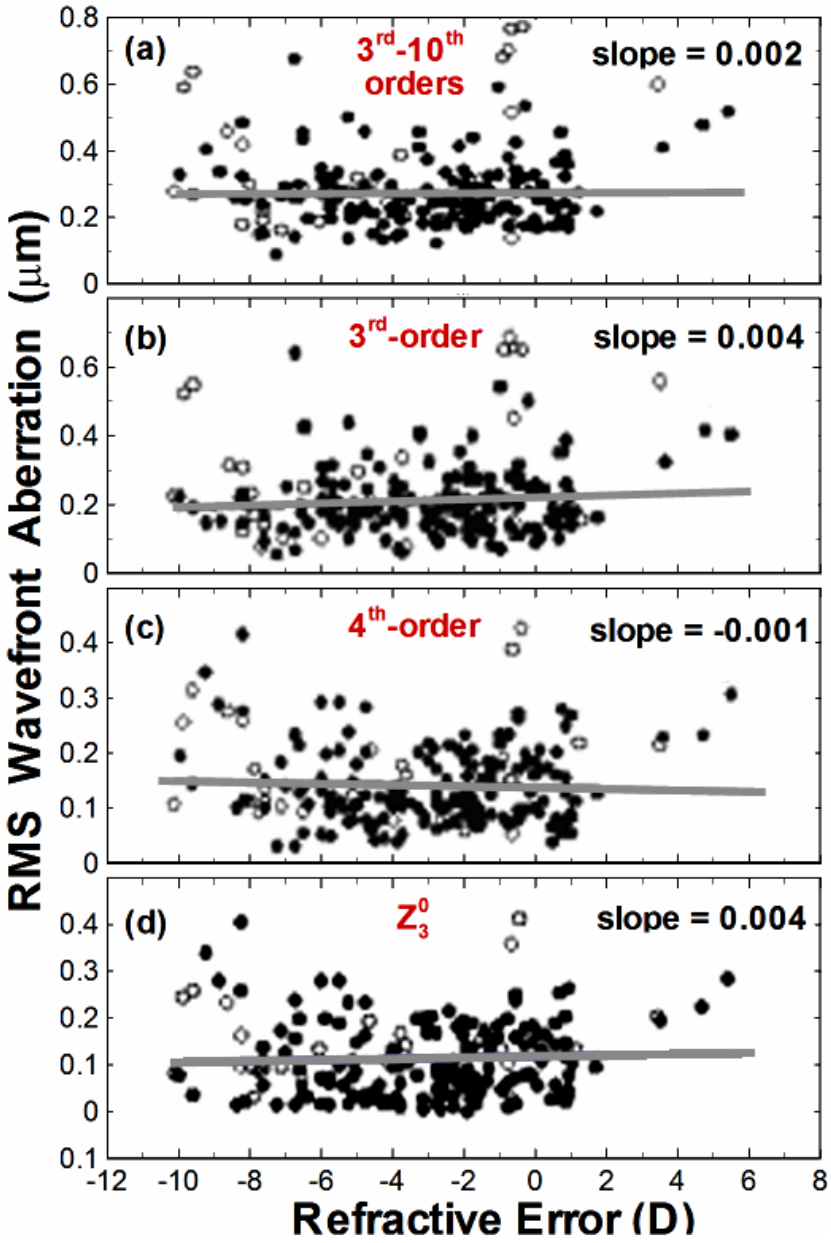

Figure 3.12 Scattergrams of RMS aberrations as functions of mean spherical equivalent refractive error. (A) total RMS error (Zernike orders 3-10), (B) third-order RMS error, (C) fourth-order RMS, (D) spherical aberration RMS error. Filled dots show data from non-astigmatic eyes (cyl < -1D), circles show data from highly astigmatic eyes (cyl >-1D), straight lines show results of linear regression. Regression slope is indicated next to each data set. [Cheng (2003)]

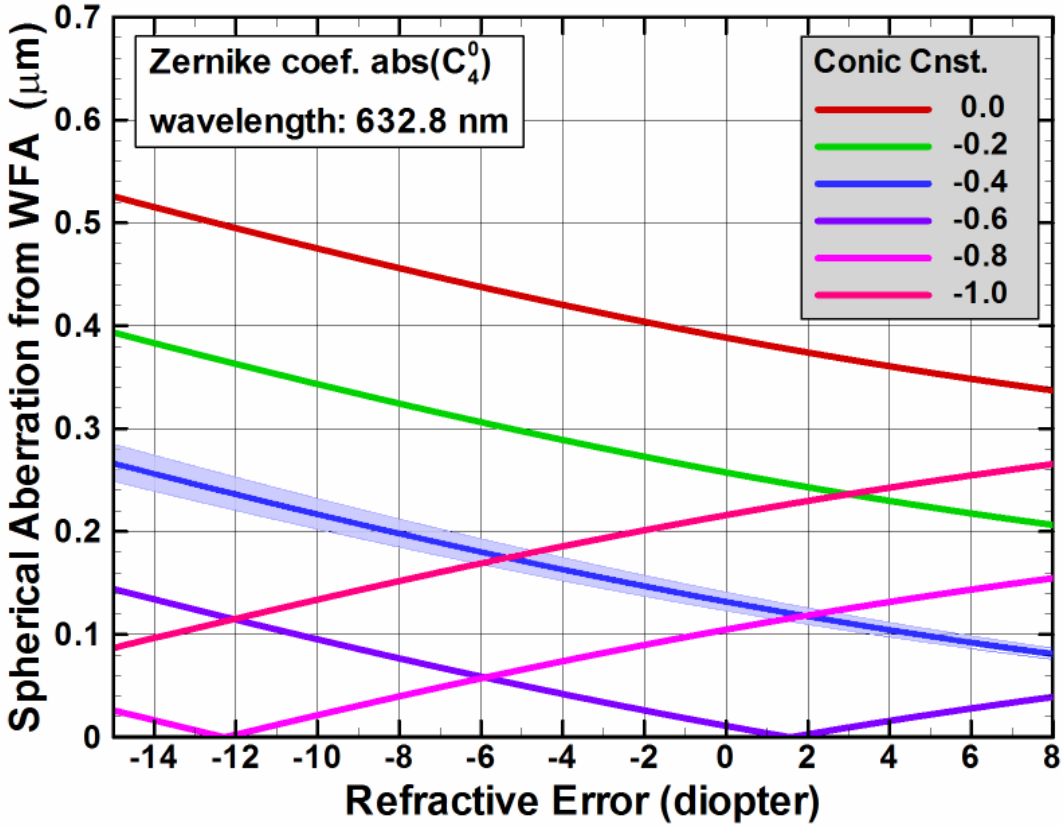

Figure 3.13 RMS of the C_4^0 wavefront aberration of general ametropic eye model

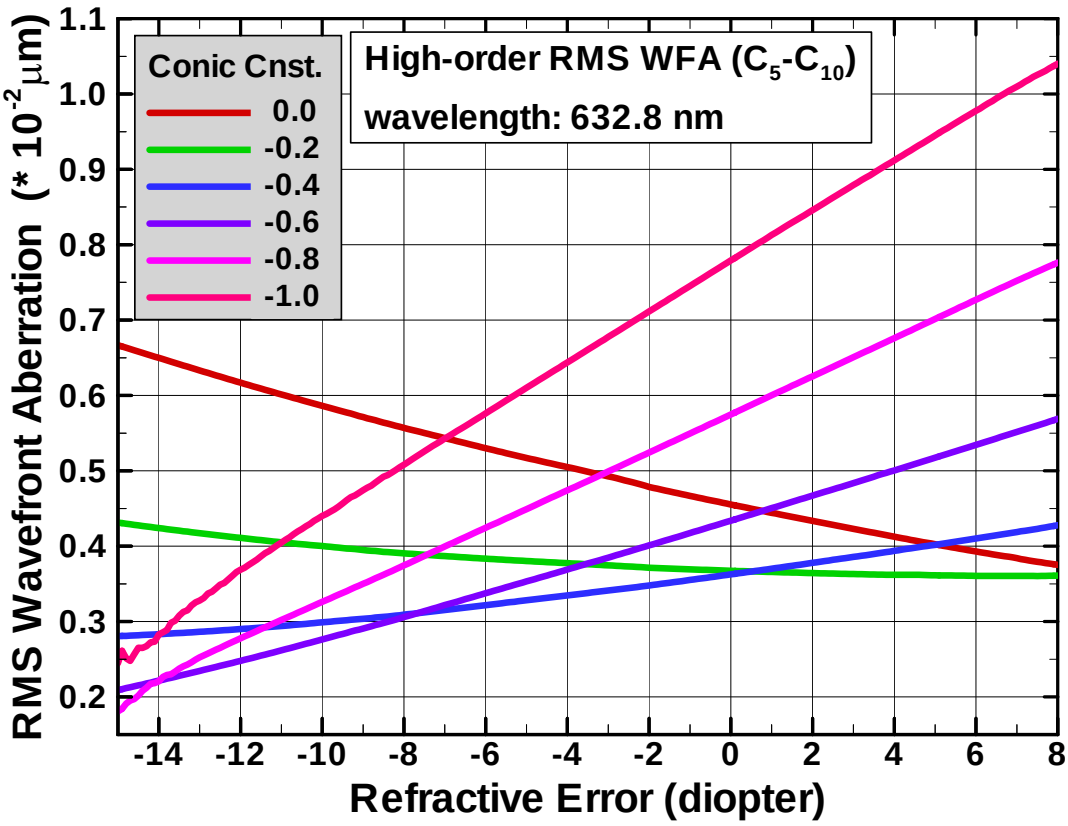

Figure 3.14 5th to 10th-order RMS wavefront aberration of general ametropic eye model

Seidel Aberration and in chapter 2. It is noticeable in Figure 3.12 that for uncorrected SA (positive Seidel SA or $Q > -0.6$) cases, slopes of the refractive-correlation are negative and for over-corrected SA (negative Seidel SA or $Q < -0.8$) the slopes turn to positive. Similarly, in Figure 3.14, the slopes of refractive correlation change sign when the wavefront deviation change from positive to negative in high orders (5^{th} – 10^{th}) in this eye model.

Since the eye models are rotationally symmetric the azimuthally dependent Zernike coefficients ($C_{n=odd}^{m}$ as well as $C_{n=even}^{m\neq 0}$) are zero. The existing terms in high-order aberrations (HOA) are therefore C_4^0, C_6^0, C_8^0, and C_{10}^0 etc. Figure 3.13 shows the non-zero spherical aberration term $\sqrt{(C_4^0)^2}$ that is comparable to measured data in Figure 3.12(D). The light blue band around the blue line of $Q = -0.4$ mark the 50% distribution of axial-length and cornea curvature variations in ametropic eyes.

As Figure 3.12(D) shows, the spherical aberration of the selected young adult population have $\sqrt{(C_4^0)^2}$ value ranged from 0 to 0.4 μm with an average at about 0.12 ±0.08 μm and a positive regression slope of 0.004 μm/diopter. For the general ametropic model eye, Zernike spherical aberration greatly depends on the cornea Q number. Comparing to the measured result, the range of 4^{th}-order aberration is predicted. However, the positive slope from measured data seems to suggest that Q distribution in the selected group of subjects are between -0.5 and -0.9 where the positive slope is possible and average aberration is around 0.1 μm. However, if the Q distribution of adults subjects is ranged between -0.1 and -0.5 as suggested in Seidel spherical aberration section (Figures. 3.5 and 3.6) value of $\sqrt{(C_4^0)^2}$ would distribute between 0 and 0.45 μm with average > 0.2 μm and has a monotonic reducing correlation with negative slope of ~

-0.007 to -0.008 since Q has none or very limited correlation with refractive error (see Figures 2.7, 2.9, and 2.10). The disagreement of correlation slope here is not initiated from the eye model but from the controversies of spherical aberration measurements using direct longitudinal SA method [Ames (1921), Koomen (1949), Jenkins (1963), Van Meeteren (1974) and Thibos (1997)] and using experimental wavefront aberration [Liang97, Marco98, Navarro97, etc.]. The measurement in the former groups tend to obtain a larger SA value (implying Q range of -0.1 ~ -0.5) and the later, a relatively smaller SA values (Q range of -0.4 ~ -0.8). If the measured SA from wavefront aberration method is adopted for model eye and Q distribution of suggested from the later group is used for population, the regression slope would not be warranted to be negative.

The remaining non-zero higher order RMS wavefront aberrations of the model eye, C_6^0, C_8^0, and C_{10}^0, are shown in Figure 3.14. The magnitude of this part of aberration obtained from eye model is in the range of 10^{-2} to 10^{-3} μm. The measured data in Figure 3.12(A) gives the high-order *RMS_W* from 3rd- to 10th-orders. The average number of all subjects is read ~0.28 ±0.08 μm. By subtracting the 3rd- (~ 0.24 μm, Figure 3.12(B)) and and 4th- (~0.14 μm, Figure 3.12(C)) from the total high-order *RMS_W*, the value of *RMS_W* of 5th- to 10th- order would be about $[0.28^2 - 0.24^2 - 0.14^2]^{1/2} \approx 0.035$ μm ,which is almost 10 times larger than that of the synthetic eye.

From the *RMS_W* comparison between measured data of human subjects and the calculation result from eye model, aberrations that were announced but not considered in the general eye model were revealed. The most significant character is the missing of 3rd-order *WFA* in model eye. This aberration contributes almost double in magnitude (~0.24 μm) than that of the spherical aberration (~0.12 μm). Previously, it is believed that the

on-axis optical performance of human eyes is dominant by the defocus and spherical aberration. This statement is based on the assumption of a rotationally symmetric eye system. The *WFA* measurement from Indiana University [Cheng 2003] shows a more significant contribution from the 3rd-order, the breaking of rotational symmetry, than from the spherical aberration to the on-axis vision. In the authors' opinion, the larger measured numbers of Seidel spherical aberration from direct longitudinal measurement [Ames (1921), Koomen (1949), Jenkins (1963), Van Meeteren (1974) and Thibos (1997)] is a result affected by the unexpected 3rd-order aberration. With the effect from the existing of non-rotational symmetric aberrations, Seidel astigmatism is really not predicted correctly for large field angle. The new technique of *WFA* provides a deeper insight for on-axis vision and periphery vision that benefits eye modeling.

In the 4th-order *WFA* part, the missing part in the eye model, $C_4^{\pm 4}$ and $C_4^{\pm 2}$, have a average quantity of about ~0.07 μm (by subtracting average values in Figure 3.12(D) from Figure 3.12 (C)). Although small compared to SA and the 3rd-order, it is more announced than the sum from 5th- and above orders aberrations (*~0.035* μm) for human eyes without pathology.

Chapter 4

Summary

In this thesis, a careful review of eye-modeling researches was given in chapter 1. In the first section of chapter 2, ametropic condition, the most prevalent vision defect, was introduced and the statistics related to gender, age, race, etc. was reviewed. In the rest sections of chapter 2, the detail construction of a general ametropic eye model was presented. This model is the first eye model that describes refractive error with variations of cornea curvature, axial length, and intraocular power simultaneously. It is also the first eye model that considers the distributions of these parameters' variations in a group of young adults. During the construction of eye model, a parameter that describes the periphery characteristics of arterial cornea surface, the conic constant, was kept a free variable between 0 (spherical surface) and -1.0 (parabola surface). It was found not influential to the status of refractive error since visual acuity is determined under small pupil diameter ~ 2-3 mm. To be in agreement with other published eye models, the refractive error in this thesis was determined under paraxial approximation which results to a small deviation of <0.2 diopter from the refractive error determined under pupil diameter of 2-3 mm.

In chapter 3, the optical performance of the eye model was evaluated and compared to measured data of human eyes. The most crucial optical performance is the on-axis (visual axis determined by the fovea location) vision. This was evaluated by the chromatic aberration and spherical aberration. The side-vision or periphery vision was evaluated by Seidel astigmatism up to 60 degree field angle. These comparisons showed fair agreement. The study of spherical aberration revealed the uncertain nature of conic constant. It was found to vary greatly among population within 0 and -1.0. In addition, the 4 quadrants of a human eye appeared to be different.

The wavefront aberration and Zernike analysis were introduced in the last section in chapter 3. The technique of measuring wavefront aberration of human eyes is quite recent. The measurement is mostly performed on-axis. The investigation showed that a single conic constant, even tailored to fit individual eye, can not fulfill the task in describing on-axis optical performance. The significant aberration from the 3^{rd}-order has twice the influence (in average) than spherical aberration. This implies that the rotational symmetry in all the eye models has to be broken to be able to predict the on-axis performance of human eye. A Zernike-coefficient-defined anterior cornea surface is a possible first amendment to the eye model. 3^{rd}-order, which was omitted before, is the first priority to change; 4^{th}-order is the next, and higher-order the last. Other enhancement of the eye modeling includes the use of gradient-refractive-index lens, the inclusion of pupil-size influence on center location of pupil, and the consideration of age-related high-order aberrations. The Stiles-Crawford effect of retina surface is an essential part of construction when double-path optics is considered. Finally, the computational

establishment of various abnormal eye conditions including cataract, floaters, keratoconus, etc. is the next goal.

References

- Applegate, R. A., Marsack, J. D., Ramos, R. and Sarver, E. J. (2003) Interaction between aberrations to improve or reduce visual performance. J Cataract Refract Surg. 2003 Aug; 29(8):1487-95.
- Amano, S., Amano, Y., Yamagami, S., Miyai, T., Miyata, K., Samejima, T. and Oshika, T. (2004) Age-related changes in corneal and ocular higher-order wavefront aberrations," Am. J. Ophthalmol. 137, 988-992.
- Ames, A. (1921) Proctor C. Dioptrics of the eye. J Opt Soc Am 1921; 11:22-85.
- American National Standards (2004) American National Standard for Ophthalmics —Methods for reporting optical aberrations of eyes ANSI Z80.28-2004.
- Atchison, D. A., Collins, M. J., Wildsoet, C. F., Christensen, J. and Waterworth, M. D. (1995) Measurement of monochromatic ocular aberrations of human eyes as a function of accommodation by the howland aberroscope technique. Vision Research 35, 313-323.
- Atchison, D. A. (2004) Recent advances in representation of monochromatic aberrations of human eyes. Clin Exp Optom 2004; 87: 3: 138–148.
- Carney, L. G., Mainstone, J. C. and Henderson, B. A. (1997) Corneal topography and myopia. A cross-sectional study. Invest Ophthalmol Vis Sci 1997; 38:311-20.
- Charman, W. N. and Jennings, J. A. M. (1976). Objective measurements of the longitudinal chromatic aberration of the human eye. Vision Research, 16, 999–1005.

- Chen, Y.-L., Lewis, J. W. L. and Parigger, C. (2000) Human Eye Model Effects on Digital Retinoscopic Diagnostic. In SESAPS annual meeting (Starkville, MI, DC1 2000).
- Chen, Y.-L., Tan, B. and Lewis, J. W. L. (2003) Simulation of eccentric photorefraction images. Optics Express, Vol. 11, No. 14, July 14, 2003
- Cheng, X., Bradley, A., Hong, X. and Thibos, L. N. (2003) Relationship between refractive error and monochromatic aberration of the eye. Optom Vis Sci. 2003 Jan; 80(1):43-9.
- Cheng, X., Himebaugh, N. L., Kollbaum, P. S., Thibos, L. N. and Bradley, A. (2003) Validation of a Clinical Shack-Hartmann Aberrometer. Optom. Vis. Sci. 80, 587-595.
- Collins, M. J., Wildsoet, C. F. and Atchison, D. A. (1995) Monochromatic aberrations and myopia. Vision Res. 1995 May;35(9):1157-63.
- Cornsweet, Tom. N. (1970) Visual Perception. Academic Press.
- El Hage and Berny (1973) Contribution of the crystalline lens to the spherical aberration of the eye. J Opt Soc Am. 1973 Feb; 63(2):205-11.
- Farrell, R. J. and Booth, J. M. (1984) Design handbook for imagery interpretation equipment. Boeing Aerospace Co., Seattle, WA, Sec. 3.2, p. 8.
- Goss, D. A., Van Veen, H. G., Rainey, B. B. and Feng, B. (1997) Ocular components measured by keratometry, phakometry, and ultrasonography in emmetropic and myopic optometry students. Optom Vis Sci 1997; 74:489-95.

- Greivenkamp, J. E. Ph. D., Schwiegerling, J. M.S., Miller, J. M. M.D., and Mellinger, M. D. M.S. (1995) Visual Acuity Modeling Using Optical Raytracing of Schematic Eyes. American Journal of Ophthalmology 1995; 120; 227-240
- Guirao, A and Williams, D. R. (2003) A method to predict refractive errors from wave aberration data. Optom Vis Sci. 2003 Jan; 80(1):36-42.
- Gullstrand, A. (1909) "The optical system of the eye," Appendix 11.3. In Helmholtz, H. Von, Physiological Optics. 3rd ed. Vols 1. (Hamburg, Voss, 1909) pp. 350-358.
- He, J. C., Burns, S. A. and Marcos, S. (2000) Monochromatic aberrations in the accommodated human eye. Vision Research 40, 41-48.
- Horner, D. G., Soni, P. S., Vyas, N. and Himebaugh, N. L. (2000) Longitudinal changes in corneal asphericity in myopia. Optom Vis Sci 2000;77:198-203.
- Isabel Escudero-Sanz and Rafael Navarro (1999) Off-axis aberrations of a wide-angle schematic eye model", J. Opt. Soc. Am. A, Vol. 16, No. 8
- Jenkins, T. C. A. (1963). Aberrations of the eye and their effects on vision: Part I. The British Journal of Physiological Optics, 20, 59-91.
- Kooijman, Aart C. (1983) Light distribution on the retina of a wide-angle theoretical eye. J Opt Soc Am. 1983 Nov; 73(11):1544-50.
- Koomen, M., Tousey, R. and Scolnik, R. (1949) The spherical aberration of the eye. J. Opt. Soc. Am. A 39, 370-376.

- Kuroda, T., Fujikado, T., Ninomiya, S., Maeda, N., Hirohara, Y. and Mihashi, T. (2002) Effect of Aging on Ocular Light Scatter and Higher Order Aberrations. Journal of Refractive Surgery 18, S598-602.
- Lewis, A. L., Katz, M. and Oehrlein, C. (1982) A modified achromatizing lens. Am. J. Optom. Physiol. Opt. 59,909-911.
- Liou, H. L. and Brennan, N. A. (1997) Anatomically accurate, finite model eye for optical modeling. J. Opt. Soc. Am. A, **14**, 1684-1695.
- Llorente, L., Barbero, S., Cano, D., Dorronsoro, C. and Marcos, S. (2004) Myopic versus hyperopic eyes: axial length, corneal shape and optical aberrations. Journal of Vision 4, 288-298.
- Lyle, W. M. (1971) Changes in corneal astigmatism with age. Am. J. Optom. Arch. Am. Acad. Optom. 48, 467-478
- Le Grand, Y. (1980) T. 1. Dioptrique de l'oeil er sa correlations. Optique physiologique, English translation by El Hage SG., Berlin, Springer-Verlag, 64-7.
- Mainstone, J. C., Carney, L. G., R., A. C., Clem, P. M., Stephensen, A. L. and Wilson M. D. (1998) Corneal shape in hyperopia. Clinical and Experimental Optometry 1998; 81:131 - 7.
- McLellan, J. S., Marcos, S. and Burns, S. A. (2001) Age-related changes in monochromatic wave aberrations of the human eye. Investigative Ophthalmology & Visual Science 42, 1390-1395.
- Meyer-Arendt, J. R. (1995) Introduction to Classical and Modern Optics, 4th Ed., Prentice-Hall, Inc., 1995.

- Navarro, R., Santamaría, J. and Bescós, J. (1985) Accommodation-dependent model of the human eye with aspherics. J. Opt. Soc. Am. A, 2, 1273-1281.
- Popiolek-Masajada, A. and Kasprzak, H.T. (1999) A new schematic eye model incorporating accommodation. Optom Vis Sci 1999 Oct;76(10):720-7.
- Rainer, G. D., Walter, A. H. and Gregor, K. E. (1998) Accurate computation of mean power and astigmatism by means of Zernike polynominals. J. Opt. Soc. Am. A/ Vol. 15, No. 6.
- Saunders, H. (1986) A longitudinal study of the age dependence of human ocular refraction – I. Age-dependent changes in the equivalent sphere. Ophthal. Physiol. Opt., 6, 39-46.
- Schwiegerling, J. T., Greivenkamp, J. E. and Miller, J. M. (1995a) Representation of videokeratoscopic height data with Zernike polynomials. Vol. 12, No. 10/ October 1995/J. Opt. Soc. Am. A
- Schwiegerling, J. T. (1995b) Visual Performance Prediction Using Schematic Eye Models.
- Shoemaker, J. A. (2002) Vision Problems in the U.S. ----Prevalence of Adult Vision Impairment and Age-Related Eye Disease in America.
- Slataper, F.J. (1950) Age norms of refraction and vision. Archs Ophthal., N.Y., 43, 468-481.
- Sorsby, A., Sheridan, M. and Leary, G.A. (1960) Vision, visual acuity, and ocular refraction of young men.", Br. Med. J., 1, 1394-1398

- Sorsby, A., Benjamin, B. and Sheridan, M. (1961) Refraction and its components during the growth of the eye from the age of three. Spec. Rep. Ser. Med. Res. Coun., No. 301. London: HMSO.
- Sorsby, A. and Leary, G. A. (1969) A longitudinal study of refraction and its components during growth. Spec Rep Ser Med Res Counc 1969;309:1-41.
- Stenström, S. (1946) Untersuchungen über die Variation und Kovariation der optischen Elemente des menschlichen Auges. Acta Ophthal., suppl. 26. (Also English translation by Woolf, D., Am. J. Optom., 25, 218-232, 1948)
- Strang, C., Winn, B. and Bradley, A. (1998) The role of neural and optical factors in limiting visual resolution in myopia. Vision Research 38, 1713–172.
- Strömberg, E. (1936) Ueber Refraction und Achsenlänge des menschlichen Auges. Acta Ophthal., 14, 281-293
- Thibos, L. N., Ye, M., Zhang, X. and Bradley, A. (1992) The chromatic eye: a new reduced-eye model of ocular chromatic aberration in humans. Applied Optics, Vol. 31 Issue 19 Page 3594
- Thibos, L. N., Ye, M., Zhang, X. and Bradley, A. (1997) Spherical aberration of the reduced schematic eye with elliptical refracting surface," Vis. Sci. 74, 548-556.
- Thibos, L. N. and Bradley, A. (1998) Modeling the refractive and Neurosensor systems of the eye, an invited chapter in "Visual Instrumentation, Optical Design and Engineering Principles." edited by Professor Zakos Mouroulis, McGraw-Hill, NewYork.

- Thibos, L. N., Applegate, R. A., Schwiegerling, J.T. and Webb, R.; VSIA Standards Taskforce Members. Vision science and its applications (2002) Standards for reporting the optical aberrations of eyes. J. Refract Surg. Sep-Oct;18(5):S652-60.
- Van Meeteren, A. (1974) Calculations on the optical modulation transfer function of the human eye for white light. Opt. Acta, 21, 395412.
- Villegas, E. R., Carretero L. and Fimia A. (1996) Le Grand eye for the study of ocular chromatic aberration. Ophthalmic Physiol Opt 1996 Nov;16(6):528-31.
- Von Helmholtz , H. (1909) Physiological Optics. 3rd ed. Vols 1 and 2. Hamburg, Voss, 91-121.
- Wald, G. and Griffin, D. R. (1947) The change in refractive power of the human eye in dim and bright light. J. Opt. Soc. Am. 37, 321-336.
- Wang, L. and Koch, D. D. (2003) Ocular higher-order aberrations in individuals screened for refractive surgery. J. Cataract Refract Surg. 29, 1896-1903.
- Zhu, L., Bartsch, D. U., Freeman, W. R., Sun, P. C. and Fainman, Y. (1998) Modeling human eye aberrations and their compensation for high-resolution retinal imaging. Optom Vis Sci. 1998 Nov;75(11):827-39

Appendix

List of technical terms and their definitions

Non-cycloplegic measurement

The measurement without paralyzing the ciliary muscle (and either the iris sphincter).

Paraxial optical description

The optical description within the central region around the optical axis where Gaussian optics is applied.

Ganzfeld luminance field

Ganzfeld, originally from German, means "whole field". Ganzfeld luminance field, especially in the optometry, means the homogeneous visual and auditory illuminates the entire retina

Accurate to the first order

Accurate under paraxial (small pupil) condition

Stiles-Crawford effect

The Stiles-Crawford effect states the directional sensitivity of both absorption and diffusive scattering on the retina. Rays of light passing through the centre of the pupil are less sensitive to the photo-sensors than rays through peripheral areas of the pupil.

Seidel aberration

The five primary aberrations of a lens system as outlined by L. von Seidel in 1885. They include spherical aberration, coma, astigmatism, curvature of field, and distortion .

Diopter (reciprocal of distance)

Unit of power of optical elements.

Snellen acuity

Visual acuity is the eye's ability to detect fine details and is the quantitative measure of the eye's ability to see an in-focus image at a certain distance. The standard definition of normal visual acuity (20/20 or 6/6 vision) is the ability to resolve a spatial pattern separated by a visual angle of one minute of arc. Visual acuity is often measured by an optometrist with the help of a Snellen chart. In the most familiar acuity test, a Snellen chart is placed at a standard distance, twenty feet in countries where that is the customary unit of measure. At this distance, the symbols on the line representing "normal" acuity subtend an angle of five minutes of arc, and the thickness of the lines and of the spaces between the lines subtends one minute of arc. This line, designated 20/20, is the smallest line that a person with normal acuity can read at a distance of twenty feet.

Exit pupil

Entrance pupil is the apparent size of the limiting aperture of a lens or lens system (properly that of the diaphragm), as seen from the object plane. The exit pupil of a lens or lens system is an image of the entrance pupil (hence conjugate to it) and normally should be the image of the limiting diaphragm. (Diaphragm is a mechanical device in a camera that controls size of aperture of the lens.)

Keratoconus eyes

Keratoconus, meaning “cone shaped,” describes a condition in which the cornea becomes thin and protrudes. This abnormal shape can cause serious distortion of visual images.

Vita

Bo Tan was born in Tianjin, China on June 30th, 1979. He was raised and studied in Tianjin until he graduated from his high school, Tianjin Yaohua High School in 1997, when he entered his undergraduate university, University of Science and technology of China, in Hefei, Anhui Province. Many of his families are teachers. Growing in this environment, he has been interested in nature and science since his childhood. His interest was developing quickly since he had his first physics course at his second year of junior middle school. This strong interest went through his middle school period and made him decide to continue the study of physics at his undergraduate university. After graduated from undergraduate with his bachelor degree of science in 2002, Bo accepted a Graduate Research Assistantship at The University of Tennessee Space Institute.